Atmos. Chem. Phys. Discuss., 8, 9347–9404, 2008
www.atmos-chem-phys-discuss.net/8/9347/2008/

Atmospheric
Chemistry
and Physics
Discussions

Sulfur isotope analyses of individual aerosol particles in the urban aerosol at a central European site (Mainz, Germany)

B. Winterholler[1], P. Hoppe[1], J. Huth[1], S. Foley[2], and M. O. Andreae[3]

[1]Particle Chemistry Department, Max Planck Institute for Chemistry, P.O. Box 3060, 55020 Mainz, Germany
[2]Department of Mineralogy, Johannes Gutenberg University, Joh.-J.-Becher-Weg 21, 55099 Mainz, Germany
[3]Biogeochemistry Department, Max Planck Institute for Chemistry, P.O. Box 3060, 55020 Mainz, Germany

Received: 4 March 2008 – Accepted: 17 March 2008 – Published: 23 May 2008

Correspondence to: B. Winterholler (winterho@mpch-mainz.mpg.de)

Published by Copernicus Publications on behalf of the European Geosciences Union.

Abstract

Sulfur isotope analysis of atmospheric aerosols is a well established tool for identifying sources of sulfur in the atmosphere, estimating emission factors, and tracing the spread of sulfur from anthropogenic sources through ecosystems. Conventional gas mass spectrometry averages the isotopic compositions of several different types of sulfur aerosol particles, and therefore masks the individual isotopic signatures. In contrast, the new single particle technique presented here determines the isotopic signature of the individual particles.

Primary aerosol particles retain the original isotopic signature of their source. The isotopic composition of secondary sulfates depends on the isotopic composition of precursor SO_2 and the oxidation process. The fractionation with respect to the source SO_2 is −9‰ for homogeneous and +16.5‰ for heterogeneous oxidation. The sulfur isotope ratio of secondary sulfate particles can therefore be used to identify the oxidation pathway by which this sulfate was formed. With the new single particle technique, different types of primary and secondary sulfates were first identified based on their chemical composition, and then their individual isotopic signature was measured separately. Our samples were collected in Mainz, Germany, in an urban environment. Secondary sulfates (ammonium sulfate, gypsum, mixed sulfates) and coatings on silicates or organic aerosol dominated sulfate loadings in our samples. Comparison of the chemical and isotopic composition of secondary sulfates showed that the isotopic composition was homogeneous, independent of the chemical composition. This is typical for particles that derive from in-cloud processing. The isotopic composition of the source SO_2 of secondary sulfates was calculated based on the isotopic composition of particles with known oxidation pathway and showed a strong dependence on wind direction. The contribution of heterogeneous oxidation to the formation of secondary sulfate was highly variable (35–75%) on day-to-day basis and depended on meteorological conditions.

1 Introduction

Particulate air pollution has been a severe problem since the onset of urbanization. Research has shown a clear connection between particulate air pollution and daily mortality (Spix et al., 1993; Pope et al., 1995; Daniels et al., 2000). EU regulations (Guideline 1999/30EG) limit the airborne particulate matter (PM_{10}) to a daily average of 50 μg m^{-3}. This limit is exceeded frequently at urban air quality monitoring stations, and legislators are planning to decrease these limits even further. Therefore, severe cuts in urban background aerosol concentrations will become necessary, and in order to devise effective control strategies, a quantitative assessment of sources is required.

Research in the Rhine-Main area (Kuhlbusch et al., 2003; Vester, 2006) and other urban areas (e.g., Lenschow et al., 2001; Pakkanen et al., 2001; Putaud et al., 2004; Puxbaum et al., 2004; Hueglin et al., 2005; Sillanpää et al., 2006; Beekmann et al., 2007) has shown that a significant portion of PM_{10} consists of secondary aerosol formed by the condensation of gaseous precursors. Sulfur dioxide, the gaseous precursor of sulfate aerosol, is released as a result of anthropogenic activity (fossil fuel and biomass burning, 60–100 Tg a^{-1}; all values expressed as mass of sulfur) and from natural sources (volcanic gases and dimethyl sulfide (DMS), 20–60 Tg a^{-1}) (Penner et al., 2001). In central Europe, stationary sources account for ca. 90% of all sulfur dioxide emissions (Lövblad et al., 2004).

Since the 1980s, the emission of SO_2 decreased drastically (~90%) in Germany, resulting in a 90% reduction of ambient SO_2 concentrations. However, these drastic cuts in ambient SO_2 concentrations did not correspond to a similar decrease in SO_4^{2-} concentrations (only ∼70% decrease). For some countries, e.g., France and the Czech Republic, observed discrepancies were even greater (~80% decrease in SO_2 and only 50% in SO_4^{2-} concentrations). The same holds for areas close to sources (i.e., urban areas; Lövblad et al., 2004). This nonlinear response of particulate sulfate concentrations to emission reductions has been widely noticed all over Europe (Irwin et al., 2002; Larssen et al., 2003; Hunova et al., 2004; Klein et al., 2004; Lövblad et al.,

Title Page
Abstract | Introduction
Conclusions | References
Tables | Figures
◀| |▶
◀ ▶
Back | Close
Full Screen / Esc
Printer-friendly Version
Interactive Discussion

2004; Fowler et al., 2005). Possible explanations are changes in oxidation patterns, deposition rates, or long range transport. Sulfur isotope ratios can be used to elucidate oxidation pathways and identify sources of sulfur in the atmosphere, and this combined information can help in understanding possible reasons for the nonlinear behavior.

In this study, we examine the chemical and isotopic composition of individual aerosol particles collected in Mainz, Germany, using the Cameca NanoSIMS 50 ion microprobe to elucidate sources and oxidation processes of sulfur in the urban and regional atmosphere.

2 Isotope chemistry of natural and anthropogenic sulfur in continental Europe

Sulfur isotope ratios are expressed in delta notation defined according to the equation given below (VCDT: Vienna Canyon Diablo Troilite)

$$\delta^{34}\mathrm{S} = \delta^{34}\mathrm{S}_{\mathrm{VCDT}} = \frac{\left(n\left({}^{34}\mathrm{S}\right)/n\left({}^{32}\mathrm{S}\right)\right)_{\mathrm{Sample}}}{\left(n\left({}^{34}\mathrm{S}\right)/n\left({}^{32}\mathrm{S}\right)\right)_{\mathrm{VCDT}}} - 1 \quad (1)$$

$(n({}^{34}\mathrm{S})/n({}^{32}\mathrm{S}))_{\mathrm{VCDT}}$=0.044163 (Ding et al., 2001)

Primary sulfate particles, such as sea salt, mineral dust, fly ash or industrial dust are directly emitted with sulfur in the form of SO_4^{2-}. Therefore, the isotopic composition of primary sulfate particles can be interpreted directly as a source signature. Five particle types dominate primary particles: biological particles, mineral dust, industrial dust, resuspended road dust and fly ash. Sulfur in plant tissue mostly reflects the isotopic composition of the atmospheric input (dry and wet deposition), unless other sources such as artificial fertilizer or local geology dominate the sulfur input into soil (Krouse and Grinenko, 1991; Gebauer et al., 1994; Novak et al., 2000; Novak et al., 2001a; Zhao et al., 2003, Bol et al., 2005; Novak et al., 2005b). The most common sources of sulfate in mineral dust are marine evaporites. The isotopic composition depends on the geological age of the deposit and δ^{34}S varies between +10‰ and +30‰. It is impossible to distinguish industrial dust emitted during the processing of natural minerals (stone dressing, cement industry, mining of mineral fertilizer) from the isotopic composition of the deposit being industrially exploited. The largest deposits exploited in Germany have δ^{34}S of ~10‰ (Zechstein). The isotopic composition of fly ash depends on the technology applied, and δ^{34}S is generally more positive than the SO_2 emitted during the same combustion process. The isotopic composition of re-suspended road dust is expected to lie somewhere between that of primary minerals and atmospheric dry and wet deposition, which can form coatings on particles. In continental Europe the contribution of sea salt (δ^{34}S=(20.7±0.3)‰; Krouse and Grinenko, 1991) and nss-sulfate produced by the oxidation of DMS (δ^{34}S=+14‰ to +22‰; Calhoun et al., 1991; McArdle and Liss, 1995; Patris et al., 2000a; Partris et al., 2000b) to the sulfur budget is negligible compared to anthropogenic emissions. In winter, the contribution of sea salt to aerosol loadings is easily overestimated due to re-suspension of road salt.

Secondary sulfates are formed by the oxidation of SO_2 and the oxidation process alters the isotopic signature (Thode et al., 1945; Eriksen, 1972a; Eriksen, 1972b; Saltzman et al., 1983; Tanaka et al., 1994). The isotopic fractionation during the gas phase oxidation of SO_2 by OH is −9‰ (Saltzman et al., 1983; Tanaka et al., 1994). The ^{34}S/^{32}S fractionation during heterogeneous oxidation is +16.5‰ (Eriksen, 1972a; Eriksen, 1972b). This shift in the sulfur isotope signature of secondary sulfate can be used to study oxidation pathways (Fig. 1), provided the isotopic composition of the source SO_2 is known (Tanaka et al., 1994).

In order to attribute SO_2 emissions to their source, the isotopic composition of the SO_2 sources must be known. Until the application of more advanced technology, the sulfur isotopic composition of SO_2 emitted during combustion of fossil fuel, the single most important source of SO_2 in continental Europe, reflected that of the fuel (Table 1; Buzek et al., 1991; Krouse and Grinenko, 1991; Querol et al., 2000; Bericnik-Vrbovsek et al., 2002). However, the introduction of flue gas desulfurization technology changed this relationship. Before the introduction of this technology, Pichlmayer et al. (1998) reported an isotopic composition of $\delta^{34}S_{SO4}$=+6‰, similar to that of the coal ($\delta^{34}S_{coal}$=~+8‰) for emissions from coal burning in Poland. In contrast, $\delta^{34}S$ of SO_2 emissions from a Polish power plant employing flue gas desulfurization technology is 13‰ more negative than the coal used in the combustion processes ($\delta^{34}S_{coal}$=~+8‰, $\delta^{34}S_{SO_2\ emissions}$=~−5‰; Table 1: Derda and Chmilewski, 2003). As a result of the widespread use of flue gas desulfurization, the isotopic composition of the fuel can no longer be used as an indicator of the source signature of anthropogenic SO_2. Instead, the isotopic composition of gaseous emissions needs to be characterized directly at the source.

3 Methods

3.1 Sample collection and site description

Samples were collected approximately 20 m above ground level, on the rooftop of the Max Planck Institute for Chemistry on the campus of the University of Mainz (49°59′31″ N, 8°14′15″ E) in August 2005 (Table 2). Fields and gardens are located to the west, while the city of Mainz and the urban Rhine-Main area are located to the east of the sampling site (Fig. 2). A municipal garbage combustion plant emitting ~25 mg of SO_2 per m^3 of flue gas is located 4 km north of the sampling site. Industrial activity is located mainly along the Rhine River to the north and east of the sampling site. Several measurement stations monitor the air quality in the city, including meteorological data as well as measurements of SO_2, O_3, $PM_{2.5}$, PM_{10} and soot, to which our data can be compared (Fig. 2; Table 3; Landesamt für Umwelt, 2005).

Samples were collected on gold coated 47-mm-diameter Nuclepore® polycarbonate filters with 0.4 μm pore sizes. After sample collection, the filters were placed in individual Petri-slides, wrapped in aluminum foil and stored in a desiccator.

Backward trajectories were calculated using the vertical motion model in the HYSPLIT4 (HYbrid Single-Particle Lagrangian Integrated Trajectory) program (Draxler and

Hess, 1998; Draxler and Rolph, 2003) with the FNL meteorological database at NOAA Air Resources Laboratory's web server (Draxler and Rolph, 2003). Back trajectory calculations were started 10 m above ground level (Fig. 3).

3.2 Classification of particles based on chemical composition

Prior to ion microprobe analysis, the samples were characterized by scanning electron microscopy (LEO 1530 FESEM) operating at an accelerating voltage of 10 keV, equipped with an Oxford Instruments ultra-thin-window energy-dispersive x-ray (EDX) detector to characterize the chemical composition, size and shape of each individual grain. These measurements were done in an automated procedure in which individual filters were scanned with 6000x magnification. The area of each particle was estimated from the number of pixels it occupied in the digital secondary electron image. The equivalent diameter was calculated as the diameter of a spherical particle occupying the same area as the analyzed particle. Only particles with an area >80 pixels were considered for sizing to ensure good accuracy for the estimated equivalent diameter (Gwaze et al., 2006). The size cut of is 1 μm (pixel size 111 nm). In order to retrieve the volume and mass of particles, the height of the particles was ascertained. Particles typically lie on their flat side. Therefore, the height of larger particles was much less than the 2-D diameter. Based on manual analysis of numerous particles, the typical height was determined to be half the 2-D diameter for particles 1 μm<x<5 μm. The average height of particles >5 μm did not exceed 2 μm.

The approximate composition of each particle was estimated based on an EDX analysis of seven of the following elements: C, N, Na, Mg, Si, P, S, Cl, K, Ca and Fe. The energy windows were chosen for each sample individually, based on the elements with the highest abundance in the sample. The X-ray spectra were acquired for predefined equidistant spots (10 μm). The acquisition time was fixed at 2 s.

Sampling regular or random spots is an established method to quantify the phase composition of samples (Amelinckx et al., 1998). To avoid multiple sampling of the same particle, the distance between the spots has to be greater than the diameter of the largest particle. Whenever this criteria is fulfilled, the probability of acquiring an EDX spectrum of a particle of particular size and chemical composition is directly proportional to the total filter area covered with particles of that size and chemical composition and, therefore, to the 2-D-surface area of the particle and number of the particles. X-ray spectra of a regular 10 μm grid were obtained, however to fulfill the above mentioned criteria the grid chosen for data analysis was varied according to the particle size analyzed. The grid chosen for data analysis was 10 μm for particles $<$10 μm in diameter, 20 μm for particles between 10 μm and 19 μm in diameter and 50 μm for particles $\geq$20 μm in diameter. Particles $\geq$50 μm in diameter were not present. Typically more than 500 particles of each sample were examined at a magnification of 6000x.

The background contribution of the empty filter to the EDX spectrum of individual particles was estimated for each sample and energy window separately using the upper (Q_u) and lower (Q_l) quartile values of the raw signals of that energy window by applying robust statistics as $Q_l - 1.726 \times (Q_u - Q_l) <$ filter background $< Q_u + 1.726 \times (Q_u - Q_l)$, which is equivalent to a 3 sigma outlier limit (Stoyan, 1998). The background signal was then subtracted from the particle signal.

Chemical signals of particles below the detection limit of the image analysis ($<$1 μm) were frequent. Numerous particles $>$1 μm were only identified by image analysis (based on the contrast of the SEM image). EDX analysis of these particles did not show any signal for the chosen energy channels. For the other particles, after background correction, the X-ray intensities were normalized to the sum of intensities detected for the particle. The relative intensities for the major elements detected were used as a proxy for the particle composition. Particles were classified into different groups based on their chemical composition and on the characteristics of different particle types observed in other studies (Xhoffer et al., 1991; Ebert et al., 2000; Mamane et al., 2001; Li et al., 2003; Sobanska et al., 2003; Ro et al., 2004; Niemi et al., 2005). As the main objective of this research is the analysis of sulfur isotope ratios, particles that contained sulfate were treated separately (see Sect. 4.1). Each particle chosen for sulfur isotope analysis was documented individually with a picture taken before and after analysis along with a full x-ray spectrum. Particles identified as ammonium sulfate based on the spectrum acquired during the automatic run were only documented after NanoSIMS analysis, because damage by the electron beam can alter their isotopic composition (Winterholler et al., 2008).

3.3 Isotope analysis of individual particles with the Cameca NanoSIMS 50

The sulfur isotope measurements were done with the Cameca NanoSIMS 50 ion microprobe at the Max Planck Institute for Chemistry in Mainz (Hoppe et al., 2005; Gröner and Hoppe, 2006; Hoppe, 2006). The high lateral resolution (<100 nm for Cs^+ primary ions) coupled with a high transmission of secondary ions for isotope measurements of the light-to-intermediate-mass elements and multi-collection capabilities (up to 5 isotopes can be analyzed simultaneously) make this instrument the only one capable of analyzing sulfur isotope ratios on individual aerosol particles (Winterholler et al., 2006; 2008).

The data in this study were obtained in multi-collection detector mode by sputtering the sample with a ∼1 pA Cs^+ primary ion beam focused onto a spot of ∼100 nm diameter. The primary ion beam was scanned over $2\times2\,\mu m^2$ around the center of individual grains. Each analysis consisted of integration of secondary ion signals over 1200 cycles of 1 s each, preceded by 600 s of pre-sputtering. Energy centering was used to compensate for charging. Secondary ions of $^{16}O^-$ $^{32}S^-$, $^{33}S^-$, $^{34}S^-$ and $^{36}S^-$ were simultaneously detected in five electron multipliers at high mass resolution. The detector dead time is 36 ns and the S^- count rates were corrected accordingly. Low-energy secondary ions were collected at a mass resolution sufficient to separate $^{33}S^-$ from the $^{32}SH^-$ interference. The energy slit was set at a bandpass of ∼20 eV and the transmission was set at ∼15–20% (specific setting of entrance, aperture, and energy slits). Here, we concentrate on the measured $^{34}S/^{32}S$ ratios because, due to the low isotopic abundances of ^{33}S and ^{36}S, the resulting errors of $^{33}S/^{32}S$ and $^{36}S/^{32}S$ ratios in single particles are large. The grain size and matrix dependence of the instrumental mass fractionation (IMF) were corrected based on the 2-D diameter and chemical composition measured for the respective particle in the SEM according to the method described in Winterholler et al. (2008). The instrumental mass fractionation for each session was determined using two $BaSO_4$ standards (IAEA SO-5 and SO-6, Isotope Hydrology Laboratory of the International Atomic Energy Agency, Vienna, Austria). Individual particles of both standards were put on two gold coated Nuclepore filters with the help of a micromanipulator and were analyzed along with the samples (Table 4, Fig. 4). The uncertainty of isotope measurements on individual aerosol particles is comparatively large due to a poor grain-to-grain reproducibility observed on standards (Winterholler et al., 2008). The grain-to-grain reproducibility of standard grains with identical chemical and isotopic composition is typically around 5‰ for micron-sized grains and between 2 and 5‰ for submicron-sized grains. This grain-to-grain reproducibility or residual error (σ_R) is determined by subtracting the average counting statistical error $\sigma_{P,m}$ from the standard deviation σ of the measurements performed on the $BaSO_4$ standard ($\sigma_R=\sqrt{\sigma^2-\sigma^2_{P,m}}$). While calculating the total measurement error (σ_T) of a measurement on an individual grain the residual error (σ_R) is added to the counting statistical error (σ_P) of the individual grain ($\sigma_T=\sqrt{\sigma^2_R+\sigma^2_P}$). However, the accuracy observed upon averaging measurements of several grains is typically 2‰ for standards (Winterholler et al., 2008) as well as for sea salt aerosol particles (Winterholler et al., 2006).

4 Results and discussion

4.1 Chemical analysis of aerosol particles

The approximate chemical composition of each particle was derived from the EDX spectra and used to group particles into 10 groups. Oxygen and carbon were present in the filter background and were, therefore, excluded from data analysis. Table 5 lists the semi-quantitative chemical composition of each group. Typical particles and EDX spectra of all groups except Group 9 (other particles) and Group 10 (identified by image analysis only) are shown in Fig. 5.

Sea salt particles (Group 1) were recognized by high intensities of sodium and chlorine. Sea salt particles age in the atmosphere by reaction with H_2SO_4, SO_2, HNO_3 and other nitrogen components giving rise to Cl depletion and sulfate/nitrate formation (Sievering et al., 1991; Mamane and Gottlieb, 1992; Zhuang et al., 1999; Laskin et al., 2003; Hoffman et al., 2004; Hwang and Ro, 2006; Saul et al., 2006). Aged sea salt particles were treated separately (Group 2). These particles typically contained >7.5% of sulfur and, therefore, significant amounts of non-sea-salt sulfate (nsss).

Silicon bearing particles (SiO_2>6%) with or without variable amounts of Na, Ca, K, Mg and Fe were considered to be quartz, clay or alumosilicates. Silicon bearing particles can be of natural (mineral dust, erosion of soil) as well as of anthropogenic origin (fly-ash). Both particle types were grouped into the same group (Group 3) during automated analysis but treated separately during isotope analysis. Almost all atmospheric particles can obtain a sulfur coating by condensation of SO_2 and/or H_2SO_4. Some mineral dust particles even react with sulfuric acid (Krueger et al., 2005). Silicate particles with sulfur coating were treated separately (Group 3a). In a similar manner, silicates (Si>6%) that acquired a nitrate coating (N>6%) during atmospheric processing, or were mixed with sea salt (Cl>6%) were assigned a separate group (Group 3b).

S-only particles, i.e., particles that showed no significant signal for elements other than S (S>95%) were considered to be secondary sulfates formed from gaseous SO_2, i.e., sulfuric acid or ammonium (bi)sulfate (Group 4). As oxygen was not analyzed, S was considered to be SO_4 except if it was associated with iron (FeS_2). Unfortunately, gold interferes with sulfur in the EDX spectrum, making high background correction necessary. Small S-only particles were, therefore, missed by single particle analysis. This missing fine mode ammonium sulfate was quantified during bulk analysis of the aerosol samples.

Calcium sulfate particles were identified by the absence of all elements other than

Ca and S in the EDX spectrum (Group 5). As oxygen was not analyzed, S was considered to be SO_4^{2-}. Primary gypsum particles have natural (soil, mineral dust, fractional crystallization of sea salt) as well as anthropogenic sources (flue gas desulfurization, metal and cement industry and road dust) (Hoornaert et al., 1996; Li et al., 2003). Reactions between sulfuric acid and $CaCO_3$ or Ca-feldspars can result in the formation of secondary gypsum (Foner and Ganor, 1992) on coarse mode particles. Cloud processing leads to the formation of secondary gypsum in the form of large needles (Fig. 6, Sample 8) or fine particles (Fig. 5, Gypsum) (Andreae et al., 1986).

All particles containing sulfur that could not be grouped into any of the above groups were referred to as mixed sulfates (Group 6). This group included sulfate particles with more than one cation. The most frequent particles were particles with Na and Ca or K and Ca as cations. Other particles in this group included sodium sulfate and potassium sulfate. Sulfide minerals (FeS_2) did not contribute significantly to any of our samples and were excluded from NanoSIMS analyses.

Particles with a relative relative intensities of Ca or Ca+Mg higher than 90% (Group 7) were considered to be $CaCO_3$, as oxygen and carbon were not analyzed. The sources of these particles are soil erosion and construction activities (McGee et al., 2003), limestone mining (Lei et al., 2004), cement production (Abdul-Wahab et al., 2005), flue gas desulfurization, glass and fertilizer production and metal industries (Hoornaert et al., 2003). In Mainz and Wiesbaden there are two cement production facilities, north and east of the sampling site. Limestone is mined south east and lime malm brick north of our sampling location (Fig. 2). Glass as well as fertilizer producing industries are located in Mainz, northeast of the sampling site.

Particles containing Fe>90% but no Cl, Si or S were considered to be iron oxides or oxyhydroxides, all of which are soil minerals (Group 8).

All particles that could not be classified into any of the above mentioned groups were grouped together (Group 9). These were secondary aerosol particles for which no sulfur was detected. Some were nitrates and phosphates, while for others Na, K and/or Ca were detected, but no anions. These particles might be oxides or oxyhydroxides.

Moreover, particles for which only one element was above the detection limit were assigned to this group.

Particles identified by image analysis only, but without any detectable EDX signal, (Group 10) included pollen grains and other biological particles, soot and secondary aerosol. Particles without characteristic EDX signal <1 μm were not analyzed.

The contribution of the different particle types for the different samples (Table 6) collected in August 2005, are as follows:

Sample 1 (Fig. 6, Table 6) was characterized by dried droplets and thin films often with secondary crystals in the fine mode <3 μm (Group 4, 5, 6, 9 and 10: 95%). In the coarse mode, biological particles (Group 10: 38%), and mineral dust (Group 3, 3a, 3b, 7, 8 and 9: ~50%) were present. Dried droplets, thin films and secondary crystals within droplets were assigned to Group 4, 5, 6, 9 or 10 depending on their chemical composition, mainly for the sake of instrumental mass fractionation correction during sulfur isotope analysis. However, these distinctions can be somewhat arbitrary. Different crystals formed by fractional crystallization from a droplet on the filter may require separate instrumental mass fractionation correction. Nevertheless, they impacted on the filter as one (liquid) particle. Vester (2006) assigned all these particles to one group termed "complex secondary aerosol".

Sample 2 was characterized by mineral dust (Group 3, 3a, 3b, 7 , 8: ~15%), aged sea salt (Group 2: 5%) and secondary particles (Group 4: 40%, Group 5: 4%, Group 6: 2%, Group 9: 21% and Group 10: 11%) in the fine mode (<3 μm); it contained biological particles (Group 10: 63%) and mineral dust (Group 3, 3a, 3b, 7, 8 and 9: ~20%) in the coarse mode. Dried droplets and thin films were absent in this sample and coated mineral dust particles accounted for less than 6% of all mineral dust particles.

Samples 4, 5 and 7 showed the highest contribution of mineral dust to both fine and coarse mode particle loadings. These three samples were characterized by mineral dust particles (Group 3, 3a, 3b, 7 and 8: 30–50%), secondary aerosol particles (Group 4: 5–14%, Group 5: 8–22%, Group 6:1–2%, Group 9: 17–28% and Group 10: 6–12%) and aged sea salt (Group 2: 0–6%) in the fine mode (<3 μm). Mineral dust particles (Group 3, 3a, 3b, 7, 8 and 9: 45–70%) and biological particles (Group 10: 25–45%) made up the coarse mode. Dried droplets were absent in Samples 4 and 5 and rare in Sample 7. Mineral dust particles with coatings accounted for 12–18% of all mineral dust particles.

Sample 8 was characterized by secondary particles formed during in-cloud processing, mineral dust particles (Group 3, 3a, 3b, 7 and 8: ∼30%) and biological particles/pollen (Group 10: 14%). Secondary particles formed during in-cloud processing included coarse mode ammonium sulfate (Group 4: 17%), long gypsum needles (Group 5: ∼30%) and other particles (Group 9: 10%).

Our results compare well with the results of Vester (2006) for samples collected on the rooftop of the Geosciences building on the campus of the Mainz University, about 200 m from our sampling site. For $PM_{2.5}$, Vester (2006) found predominantly "complex secondary particles" (69–83%), i.e., internal mixtures of secondary organic aerosol, ammonium sulfate and other secondary aerosol particles, aged sea salt (0–20%), soot (3–5%) and silicate and mixed silicate particles (0–6%). We found on average 71% secondary particles (Group 4, 5, 6 9 and 10), 1% aged sea salt (Group 2), and 27% mineral dust particles with and without coatings (Group 3, 3a, 3b, 7 and 8). In the size range 2.5–10 μm. Vester (2006) found aged sea salt particles (0–70%), calcium nitrate and calcium carbonate particles (0–65%), and silicate and mixed silicate particles (8–50%). In August 2005 we found secondary sulfate particles formed during wet processing (Sample 8: 46%), biological particles (Group 10: 37%), and mineral dust particles (Group 3,3a, 3b, 7 and 8: 33%). The contribution of aged sea salt to our samples was minor (0–4%).

The aerosol mass calculated from single particle analyses was compared to measurements by the state agency for environmental protection (Landesamt für Umwelt, Wasserwirtschaft und Gewerbeausicht Rheinland-Pfalz). PM_{10} is measured at several sites in Mainz by Beta-Absorption, and has been reportedly corrected to be consistent with the standard procedure DIN EN 12341 (1998), which is a gravimetric analysis at (50±5)% relative humidity and (20±1)°C after 48 h conditioning. $PM_{2.5}$ and soot are monitored only at one site (Table 3). The difference $PM_{2.5-10}$ estimated from our data agreed well with $PM_{2.5-10}$ reported for the monitoring station upwind from our sampling site (Table 3), while $PM_{2.5}$ calculated from the single particle analysis under ultra high vacuum conditions was approximately 85% lower than $PM_{2.5}$ at 50% relative humidity at the station upwind from our sampling site (Table 3). There are two reasons for the $PM_{2.5}$ estimated by single particle analysis being lower than the bulk measurements. Firstly, the automated procedure chosen for characterizing the aerosol focused on identifying sulfates for sulfur isotope analysis and missed particles $<1\,\mu$m without characteristic EDX signal, such as secondary organic aerosol and soot particles, which were not relevant for this study. Secondly, $PM_{2.5}$ at 50% RH contains water (10–30%; Hueglin et al., 2005) which is absent under the ultra high vacuum conditions during SEM analysis.

4.2 Isotopic composition of different types of sulfate aerosol particles and bulk samples

Chemical analysis of aerosol collected in Mainz led to the identification of six groups of sulfate-containing particles. The contribution of each of these groups to the sulfate content of each sample was calculated based on results from single particle and bulk analyses (Table 7). The isotopic composition of each group was measured by NanoSIMS (Table 7). Details of all analyses are listed in Table 8. Most sulfur was present in the form of secondary sulfate particles.

For five out of six samples, the isotopic composition of secondary gypsum (Group 5), mixed sulfate particles (Group 6), sulfur coatings on silicates (Group 3a) and aged sea salt (Group 2) agreed with each other within the analytical uncertainty. Thus, irrespective of the chemical composition, precursor SO_2 and oxidation process that might have lead to the formation of different secondary aerosol particles, all secondary particles show a uniform isotopic signature. This is only possible if all of these particles were formed from droplets that had been isotopically homogenized by frequent in-cloud processing. The weighted averages of particles from Groups 2, 3a, 5 and 6 were

$\delta^{34}S=(19\pm3)$‰, $\delta^{34}S=(20\pm7)$‰, $\delta^{34}S=(5\pm2)$‰, $\delta^{34}S=(14\pm2)$‰, and $\delta^{34}S=(8\pm3)$‰ for Samples 1, 2, 5, 7 and 8 , respectively. Sample 4, for which the isotopic composition of different secondary particles differed, was collected on a day with low relative humidity (Sample 4; Table 2). In Sample 4 the isotopic composition of sulfur coatings on silicates (Group 3a, $\delta^{34}S=(1\pm2)$‰) differed from the isotopic composition of secondary gypsum and mixed sulfate particles (Groups 5 and 6, $\delta^{34}S=(10\pm2)$‰). There are two explanations why the $\delta^{34}S$ of sulfur coatings on silicates was lower than that of other particles. Firstly, the contribution of heterogeneous oxidation to the formation of sulfur coatings on silicate particles might be lower. Secondly, different precursor SO_2 might have lead to the formation of these coatings.

Ammonium sulfate/sulfuric acid particles (Group 4) derive from gas to particle conversion (Group 4a) and/or in-cloud processing (Group 4b). Ammonium sulfate particles that went through in-cloud processing were assigned to Group 4b based on the following three criteria. Firstly, ammonium sulfate in the form of dried droplets was assigned to this group. Secondly, coarse mode ammonium sulfate particles (2.5–15 μm) were considered to be formed by in-cloud processing based on their large size and spherical shape. Thirdly, ammonium sulfate particles <2.5 μm were assigned to this group if their isotopic composition agreed within the analytical uncertainty with that of other secondary particles in the respective sample that were known to have been homogenized by in-cloud processing (i.e., Group 3a, 5 and 6). The isotopic composition of ammonium sulfates derived from gas to particle conversion and in cloud processing typically differed by 18‰. For particles <2.5 μm the fraction formed by gas to particle conversion (typically 65% of the total mass of Group 4) was established based on the number of ammonium sulfate particles in this size range assigned to Group 4a and Group 4b, respectively. Only the isotopic composition of particles deriving from gas to particle conversion was used to estimate the isotopic composition of source SO_2 (Fig. 1). The contribution of ammonium sulfate particles deriving from gas to particle conversion to the total sulfate mass in the sample was high (~40% of the total sulfate mass) only for Sample 2. This sample was collected on a day with low relative humidity.

Typically only <20% of total sulfate mass was found in particles deriving from gas to particle conversion only. The rest was homogenized by in cloud processing (60–95%) or was present in the form of primary sulfates. As the lifetime of SO_2 with respect to oxidation by OH is at the order of 10 d, the amount of sulfur found in particles presumably formed by gas to particle conversion might look a bit high at first sight. However, except for Sample 7, samples were collected on dry and sunny days, favoring gas-phase processes.

The isotopic composition of ammonium sulfate measured in fine mode ammonium sulfate samples ranged from $\delta^{34}S=(-16\pm5)$‰ to (2 ± 3)‰ (Table 7) for particles deriving form gas to particle conversion, and $\delta^{34}S=(1\pm4)$‰ to (19 ± 4)‰ (Table 7) for particles that went through in-cloud processing.

Gypsum particles can be of either primary or secondary origin. Primary gypsum particles were typically coarse mode particles (Fig. 5, Group 5). The isotopic composition of primary gypsum particles was $\delta^{34}S=(17\pm2)$‰ for Sample 7 and particles were associated with silicates, suggesting soil minerals as the origin of primary gypsum in this sample. The $^{34}S/^{32}S$ ratio agrees with the isotopic composition expected for soil minerals. The isotopic composition of fly ash ($\delta^{34}S_{nsss}=(25\pm5)$‰) (Fig. 7, Table 7) from a north-western wind direction indicated that the isotopic composition of gypsum formed in the fumes of this emission source cannot be distinguished from natural sources, such as fractional crystallization of sea salt or soil minerals. Primary Ca-phosphate (Sample 5) with an isotopic composition of $\delta^{34}S=(23\pm5)$‰ most likely originated from fertilizer production located north east of our sampling site. Unaltered sea salt (Group 1) particles were absent in our samples. Particles classified into this group by automated single particle analyses always showed reactions with sulfuric acid and formation of nss-sulfate upon visual inspection (e.g., the particle shown in Fig. 5, aged sea salt). The contribution by these particles to the total sulfate mass of the individual samples was minor (0–5%). The isotopic composition of aged sea salt particles was measured as $\delta^{34}S=(12\pm7)$‰ (Table 7). The isotopic composition measured on biological particles averages the isotopic composition of plant sulfur and fine mode particles or coatings on the surface of the particles, and ranged from δ^{34}S=(9±10)‰ to (26±5)‰.

The bulk isotopic composition of each sample was calculated based on the isotopic composition of each group and the fraction that it contributed to the total sulfate mass:

$$\delta^{34}\mathrm{S}_{\mathrm{bulk}} = \sum f_i \times \delta^{34}\mathrm{S}_i \qquad (2)$$

and the error of the calculated bulk composition is

$$\sigma_{\mathrm{bulk}} = \surd\left(\sum (f_i \times \sigma_i)^2\right). \qquad (3)$$

Missing measurements were taken as 0 with an error of ±20‰. This error spans the full range of values expected for anthropogenic emissions.

The δ^{34}S value of bulk sulfate in air masses reaching Mainz from the north-western direction (Sample 2, 7 and 8: $\delta^{34}\mathrm{S}_{\mathrm{nsss}}$=(13±1)‰) was higher than that of bulk sulfate in air masses reaching Mainz from an eastern direction (Samples 4 and 5: $\delta^{34}\mathrm{S}_{\mathrm{nsss}}$=(5±2)‰). Sample 1 was collected on a sunny day, in the aftermath of rainfall that occurred in the previous night, and has the lowest particle and sulfate loadings. This sample likely represents local sulfur sources and has an isotopic composition of $\delta^{34}\mathrm{S}_{\mathrm{nsss}}$=(10±2)‰.

We compared the isotopic composition of bulk samples with in situ measurements of the sulfur isotopic composition of wet deposition (Mayer et al., 1995a; Mayer et al., 1995b; Alewell and Gehre, 1999; Novak et al., 2000; Novak et al., 2001b; Knöller and Trettin, 2003; Einsiedl et al., 2007) and aerosol samples (Pichlmayer et al., 1998; Novak et al., 2000; Tichomirowa et al., 2004; Tichomirowa et al., 2007) along the path of the back trajectory. Only Pichlmayer et al. (1998) analyzed the dependence of the sulfur isotopic composition on the back trajectories of the collected samples and found a range from δ^{34}S=1–9.4‰ in aerosol samples collected on different days at Sonnblick observatory in the Alps. The observed range in the bulk aerosol samples collected in Mainz (δ^{34}S=(3±3)‰ to (14±1)‰) is similar to the range of isotope ratios observed at Sonnblick.

Title Page
Abstract
Introduction
Conclusions
References
Tables
Figures
◀◀
▶▶
◀
▶
Back
Close
Full Screen / Esc
Printer-friendly Version
Interactive Discussion

The $\delta^{34}S$ of samples reaching Mainz from an eastern direction (Samples 4 and 5, Fig. 5.3, D) is lower than the annual average $\delta^{34}S$ of aerosol particles observed in Saxony ($\delta^{34}S=10‰$; Tichomirowa et al., 2007), but well within the range of monthly average $\delta^{34}S$ reported for aerosol collected in the Czech Republic ($\delta^{34}S=3.1–16.9‰$; Novak et al., 2000), wet deposition in northern Bavaria ($\delta^{34}S=1–3‰$; Mayer et al., 1995a), the Fichtelgebirge ($\delta^{34}S=3–7‰$; Alewell and Gehre, 1999), around Leipzig ($\delta^{34}S=\sim4‰$; Knöller and Trettin, 2003), and Saxony ($\delta^{34}S=3–6‰$; Tichomirowa et al., 2007). No measurements are available for comparison with samples reaching Mainz from the north (Samples 7 and 8; Fig. 3b and c) and north west (Samples 1 and 2; Fig. 3a and b).

4.3 Isotopic composition of source SO_2

The isotopic composition of secondary sulfates depends on two factors – the isotopic composition of the source SO_2, and the oxidation process responsible for oxidizing SO_2 to SO_4^{2-}. In order to unambiguously interpret the measurements, one of these two factors needs to be known, i.e., for interpreting sulfur isotope data of secondary sulfate in terms of the source composition of the SO_2, the oxidation process needs to be known, or, alternatively, to understand the oxidation process the source composition has to be identified first.

Since in our case, both source composition and oxidation pathway are unknown, we have to make the assumption that we have correctly identified those fine mode ammonium sulfate particles that derived from gas to particle conversion as opposed to ammonium sulfate form by in-cloud processing (Table 7, Fig. 1). This assumption is justified, because our single particle data shows, that secondary sulfates that went through in-cloud processing are isotopically homogenized irrespective of their chemical composition (see Sect. 4.2). The large differences (~18‰) observed between the isotopic composition of most fine mode ammonium sulfate particles (65% of fine mode ammonium sulfate; Group 4a in Table 7) and all other secondary sulfate particles including coarse mode ammonium sulfate particles (Group 2, 3a, 4b, 5 and 6 in Table 7) is strong evidence for the fact that they were formed by different atmospheric processes. Note that particles <2.5 µm with an isotopic composition that agreed within errors with the isotopic composition of other secondary particles homogenized by in-cloud processing (∼35% of the particles in this size range) were excluded from Group 4a and assigned to Group 4b.

The OH lifetime of SO_2 is of the order of 10 d, which means that more distant sources might contribute to the H_2SO_4(g). However, due to aqueous phase oxidation and SO_2 deposition the overall lifetime of SO_2 is on the order of two days (Fig. 8) and the isotopic composition of precursor SO_2 can only be calculated for ammonium sulfate /sulfuric acid particles that have not been isotopically homogenized by inclusion into no-precipitating clouds. Therefore, the isotopic composition calculated for the precursor SO_2 is most likely influenced by local and regional sources.

The highest local SO_2 concentration was always observed at the measurement site located inside the city (Goetheplatz), northeast of our sampling site, pointing towards the existence of SO_2 sources inside the city. Previous research in Antwerp and Munich showed that the isotopic composition of SO_2 at an urban site is controlled by local sources rather than long range transport (Torfs et al., 1997, Mayer et al. 1995a).

Sample 1 has the lowest sulfate content of all samples. This sample was collected from 2 August 16:00 UT+2 to 3 August 15:00 UT+2. As it rained from 1 August into the early morning hours of 2 August the air was very clean. However, sunny conditions prevailed during most of 2 August and on 3 August, facouring gas to particle conversion. The isotopic composition calculated for the source SO_2 of this sample was $\delta^{34}S=(-7\pm6)$‰.

The isotopic composition estimated for the source SO_2 of samples reaching Mainz from eastern directions was $\delta^{34}S=(-1\pm2)$‰ and $\delta^{34}S=(-6\pm2)$‰ for Sample 4 and 5, respectively ($\delta^{34}S_{SO_2}$ in Table 7). The isotopic composition of SO_2 measured at different locations east of our sampling site ($\delta^{34}S=1$–3‰; Gebauer et al., 1994; Tichomirowa et al., 2007; Novak et al., 2001b) is generally higher than the isotopic composition estimated for source SO_2 reaching Mainz from an eastern direction ($\delta^{34}S=(-2\pm2)$‰). However, similar low isotope ratios have been observed at urban locations in Munich (Mayer et al., 1995b), Antwerp (Torfs et al., 1997) and Braunschweig (Jäger et al., 1989), and the urban area of Rhine-Main is located east of our sampling site.

The isotopic composition for SO_2 reaching Mainz from northern direction was $\delta^{34}S=(11\pm2)$‰. The source of these emissions is unknown, but a municipal waste incineration plant is located north of our sampling site. Nevertheless, more distant sources such as large stationary sources in the Ruhr area, over which the back trajectories of the samples passed must also be considered. Over all the isotopic composition of SO_2 reaching the sampling site shows a clear dependence on wind direction (Fig. 9).

4.4 Contribution of homogeneous and heterogeneous oxidation to secondary sulfate formation in different types of aerosol particles

As the objective of this work is to understand the formation process of secondary sulfate aerosol, primary sulfate and secondary sulfate must be treated separately. Non-soluble primary particles such as primary gypsum particles (mineral dust, industrial dust and fly ash) and plant fragments are identified based on morphology and sulfur in such particles is neglected for the present analysis. These particles are typically not water soluble and, therefore, not internally mixed with secondary sulfate. The main source of water soluble primary sulfate is sea salt. Sea salt sulfate can be internally mixed with secondary sulfate. For the particle collected in Mainz this is the case mainly in aged sea salt particles. The nss-sulfate content (= the secondary sulfate content) of aged sea salt was calculated based on the Cl and SO_4^{2-} content of aged sea salt particles measured during single particle analysis. (Sea-salt sulfate=Cl×0.14, Non-sea-salt sulfate=$SO_4^{2-}-(Cl\times0.14)$, 0.14 is the weight ratio between sulfate and chlorine in sea water, f_{nsss}=nsss/(sss+nsss), Krouse and Grinenko, 1991). For aged sea salt particles, the sea salt sulfate (primary sulfate) with an isotopic signature of 20.7‰ has to be subtracted from the δ^{34}S in order to calculate the isotopic composition of the non sea salt sulfate (secondary sulfate), $\delta^{34}\mathrm{S}_{\mathrm{nsss}}$ ($\delta^{34}\mathrm{S}_{\mathrm{particle,nsss}}=\delta^{34}\mathrm{S}_{\mathrm{particle}}-f_{\mathrm{sea\ salt}}\times 20.7$). The sea salt sulfate content of most of the secondary sulfate containing particles (Groups 3a, 4a, 4b, 5 and 6, Table 5) was negligible ($\delta^{34}\mathrm{S}_{\mathrm{nsss}}\sim\delta^{34}\mathrm{S}$). Therefore, no subtraction of sea salt sulfate was necessary ($\delta^{34}\mathrm{S}_{\mathrm{nsss}}\sim\delta^{34}\mathrm{S}$).

The contribution of heterogeneous oxidation to the formation of secondary sulfate in particles of Group 2, 3a, 4a, 4b, 5 and 6 was calculated according to the formula

$$f_{i,\mathrm{het}} = (\delta^{34}\mathrm{S}_{\mathrm{nsss},i} - \delta^{34}\mathrm{S}_{4a})/(0.0257\times(1+\delta^{34}\mathrm{S}_{4a})). \tag{4}$$

for each of the groups separately. $f_{\mathrm{nsss},i}$ is calculated based on the chemical composition of the particles presented in Table 5.

The error is

$$\sigma_{f\,i,\mathrm{het}} = \sqrt{}(\sigma^2_{\mathrm{nsss},i} + \sigma^2_{4a})/(0.0257\times(1+\delta^{34}\mathrm{S}_{4a})). \tag{5}$$

The isotopic composition of fine mode ammonium sulfate particles that have not been homogenized by in-cloud processing (Group 4a) is considered to represent the isotopic composition of particles derived from homogeneous oxidation only. Assuming a fractionation in the δ^{34}S of +16.5‰ with respect to the source $\mathrm{SO_2}$ for the heterogeneous oxidation pathway and −9‰ with respect to the source $\mathrm{SO_2}$ for the homogeneous oxidation pathway, the maximum difference between the two pathways is 25.7‰. The contribution of heterogeneous oxidation to the total secondary sulfate was based on the contribution of heterogeneous oxidation to the secondary sulfate on the individual group e.g. group 5, and the fraction that each group contributed to the total nss-sulfate content of the sample

$$f_{\mathrm{secondary,het}} = \Sigma(f_{\mathrm{secondary},i}\cdot f_{i,\mathrm{het}}). \tag{6}$$

The error of the estimate is

$$\sigma_{\mathrm{secondary,het}} = \sqrt{\left[\Sigma(f_{i,\mathrm{secondary}}\times\sigma_{f\,i,\mathrm{het}})^2\right]} \tag{7}$$

As particles in group 4a derive from homogeneous oxidation only, $\sigma_{4a,\mathrm{het}}$ is 0 by definition.

The contribution of heterogeneous oxidation to secondary sulfate formation ranges from ~42% to ~82%. Within the individual samples, the isotopic composition of particles from Group 3a, 4b, 5 and 6 agrees within the 2σ analytical uncertainty. Therefore, the average contribution of heterogeneous oxidation to the formation of different secondary particles is roughly similar (secondary gypsum: (75±10)%, sulfur coatings on silicates: (54±9)%, coarse mode ammonium sulfate: (71±8)%, and mixed sulfate particles: (71±10)%). In contrast, the difference between the contributions of heterogeneous oxidation to particles homogenized by in-cloud processing (Group 2, 3a, 4b, 5 and 6) in different samples is more pronounced (Sample 1: (128±27)%, Sample 2: (71±33)%, Sample 4: (66±14)%, Sample 5: (72±27)%, Sample 7: (47±16)%).

Including Group 4a, the contribution of heterogeneous oxidation to the formation of secondary sulfates was (102±26)%, (42±24)%, (60±15)%, (71±28)% and (44±16)% for Sample 1, Sample 2, Sample 4, Sample 5 and Sample 7, respectively. The highest contribution of heterogeneous oxidation was found in Sample 1, which was collected following a rainfall event, and Sample 5. Both samples experienced nighttime relative humidity of ~95%. The lowest contribution of heterogeneous oxidation was observed for a sample collected on a day when the nighttime relative humidity was low (~80%, Sample 2, Table 2).

In order to establish whether the nonlinear response to emission reductions coincided with a change in the relative contribution of the homogeneous and heterogeneous oxidation pathways to the formation of secondary sulfates, we compare our data to previously reported results. Current atmospheric chemistry models suggest that 24–56% of precursor SO_2 is removed by dry and wet deposition before oxidation and only 42–82% of precursor SO_2 is oxidized (Penner et al., 2001, Fig. 8). Of the SO_4^{2-} formed by oxidation of SO_2, 64–90% is formed by aqueous oxidation and 10–36% by homogeneous oxidation. The contribution of heterogeneous oxidation to the formation of secondary sulfates can be estimated by simultaneous measurements of the isotopic composition of SO_2 and SO_4^{2-} (Tanaka et al., 1994). Querol et al. (2000) measured the S isotope fractionation between the SO_2 emitted by a coal fired power plant in Spain and the SO_4^{2-} derived from the oxidation of the SO_2. In the stack, the average difference in $\delta^{34}S$ between SO_2 and fly ash was 1.9‰, while in the plume the difference increased to 2.8‰. Numerous other observations in the 1970s and 1980s by Krouse and Grinenko (1991) showed that the oxidation of SO_2 is associated with an average $^{34}S/^{32}S$ fractionation of about +3‰ (range: −5.1–12.5‰). This implies a typical contribution of heterogeneous oxidation to the conversion of SO_2 to SO_4^{2-} of ∼43% in the stack of a combustion plant and ∼46% under ambient atmospheric conditions. In Central Europe, Mayer et al. (1995a) found no difference between the isotopic composition of SO_2 and sulfate in bulk precipitation in 1989 (∼35% heterogeneous oxidation), while Novak et al. (2001b) found an average difference of 4.1‰ between the isotopic composition of SO_2 and SO_4^{2-} at several sites in the Czech Republic (averaged over the years 1992 to 1997) pointing towards ∼50% contribution of heterogeneous oxidation to the formation of sulfate.

The average differences between the $\delta^{34}S$ values of SO_2 and SO_4^{2-} observed in all these previous studies were lower than the average differences between SO_2 and SO_4^{2-} in our samples collected in August 2005 ((6.7±2.4)‰). However, our results compare well with recent measurements by Tichomirowa et al. (2007), who found an average difference of 6.6‰ and 9.3‰ between the isotopic composition of SO_2 and aerosol samples at two sites in Saxony (averaged over the years 1997 to 2004). Both results support an increase in the contribution of heterogeneous oxidation to the formation of sulfate from a typical contribution of ∼46% in the 1970s and 1980s to approximately 60–70% in recent years. Nevertheless, the fraction of aqueous phase oxidation estimated by the study of sulfur isotope ratios is at the lower end of the contribution of aqueous phase oxidation estimated by atmospheric chemistry models.

There are two possible reasons why such an increase in the efficiency of the heterogeneous oxidation pathway is the most likely explanation for this shift in the relative contribution of both oxidation pathways. Firstly, the oxidation of SO_2 by ozone is strongly pH dependent and emission reductions of all major acidifying compounds have lead to a decrease in the acidity of cloud droplets and precipitation from pH 4.4 in the early 1980s to pH 4.9 from 2000 to 2004 at all EMEP measurement stations in Germany (Klein et al., 2004). This increase in droplet pH corresponds to a one order of magnitude change in the S(IV) oxidation rate by ozone (from ca. 3×10^{-10} to 3×10^{-9}; Lee and Thiemens, 2001). Secondly, median ozone concentrations have increased during the aforementioned period (Klein et al., 2004). Therefore, the nonlinear response of particulate sulfate concentration to emission reductions is not only caused by a shift from an oxidant limited system towards more complete oxidation closer to sources due to lower sulfur dioxide emissions, but also to a shift towards a higher fraction of heterogeneous oxidation. In fact, our results suggest that SO_2 emission reductions coupled with rising ozone concentrations lead to an increase in the oxidation capacity of the urban atmosphere.

5 Conclusions

The results of this study show that, despite limitations in precision, the NanoSIMS technique is a novel and useful tool for the isotope analysis of individual atmospheric particles, enabling us to compare the chemical and isotopic composition of individual aerosol particles. Given the range of S-isotopic ratios in aerosol bulk samples, the achievable precision and accuracy of a few per mil for the measurement of the $^{34}S/^{32}S$ ratio in individual aerosol particles is sufficient to investigate physical and chemical processes related to aerosol formation and transport.

We found that the isotopic composition of sulfate and SO_2 at our site depended mainly on wind direction, suggesting a dependence on local sources. Different types of secondary sulfate particles were usually isotopically homogeneous, irrespective of chemical composition, except on days with extremely low relative humidity.

The contribution of heterogeneous oxidation to the formation of secondary sulfates was estimated to be typically around 60% and showed a dependence on meteorology. The comparison of our data to previous results in Central Europe (Novak et al., 2001b, Tichomirowa et al., 2007) indicated that the estimated contribution of heterogeneous oxidation to the formation of sulfate has increased from around 50% in the early 1990s to ca. 60–70% in 2005. This shift in the relative contribution of the two major oxidation pathways coincided with a strong decrease of SO_2 emissions, and might be partially responsible for the weaker response of urban $PM_{2.5}$ concentrations to the drastic decrease in the emission of gaseous precursors.

Future studies of the mass independent oxygen isotope fractionation of sulfate particles could confirm whether changes in the contribution of ozone to sulfate formation are taking place.

Acknowledgements. This research was funded by the Max Planck Society. We thank E. Gröner for his support with the NanSIMS analyses.

References

Abdul-Wahab, S., Worthing, M. A., and Al-Maamari, S.: Mineralogy of atmospheric suspended dust in three indoor and one outdoor location in Oman, Environ. Monit. Assess., 107, 313–327, 2005.

Alewell, C. and Gehre, M.: Patterns of stable S isotopes in a forested catchment as indicators for biological S turnover, Biogeochem., 47, 319–333, 1999.

Amelinckx, S., van Dycke, D., van Landuyt, J., and van Tendeloo, G.: Handbook of microscopy: applications in materials science, solid-state physics and chemistry, Wiley-VCH, 1998.

Andreae, M. O., Charlson, R. J., Bruynseels, F., Storms, H., van Grieken, R., and Maenhaut, W.: Internal Mixture of Sea Salt, Silicates, and Excess Sulfate in Marine Aerosols, Science, 232, 1620–1623, 1986.

Beekmann, M., Kerschbaumer, A., Reimer, E., Stern, R., and Möller, D.: PM measurement campaign HOVERT in the Greater Berlin area: model evaluation with chemically specified particulate matter observations for a one year period, Atmos. Chem. Phys., 7, 55–68, 2007, http://www.atmos-chem-phys.net/7/55/2007/.

Bericnik-Vrbovsek, J., Pichlmayer, F., Blochberger, K., Jeran Z., and Marsel. J.: Isotopic analysis of sulphur in the assessment of SO_2 emission sources, Acta Chimica Slovanka, 49, 149–157, 2002.

Bol, R., Eriksen, J., Smith, P., Garnett, M. H., Coleman, K., and Christensen, B. T.: The natural abundance of ^{13}C, ^{15}N, ^{34}S and ^{14}C in archived (1923–2000) plant and soil Samples from the Askov long-term experiments on animal manure and mineral fertilizer, Rapid Comm. Mass. Sp., 19, 3216–3226, 2005.

Buzek, J., Cerny, J., and Sramek, A. G.: Sulfur isotope studies of atmospheric S and the corrosion of monuments in Praha, Czechoslovakia, in: Stable Isotopes. Natural and Anthropogenic Sulfur in the Environment. Case Studies and Potential Applications, edited by: Krouse, H. R. and Grinenko, V. A., Chichester, Wiley, 399–404, 1991.

Calhoun, J. A., Bates, T. S., and Charlson, R. J.: Sulfur Isotope Measurements of Submicrometer Sulfate Aerosol-Particles over the Pacific-Ocean, Geophys. Res. Lett., 18, 1877–1880, 1991.

Daniels, M. J., Dominici, F., Samet, J. M., and Zeger S. L.: Estimating particulate matter-mortality dose-response curves and threshold levels: An analysis of daily time-series for the 20 largest US cities, Am. J. Epidemiol., 152, 397–406, 2000.

Derda, M. and Chmielewski, A. G.: Determination of sulfur isotope ratios in coal combustion processes, Paper presented at the Sixth International Symposium & Exhibition on Environmental Contamination in Central & Eastern Europe and the Commonwealth of Independent States 1-4 September 2003, Prague, Czech Republic, 2003.

DIN EN 12341: Luftbeschaffenheit – Ermittlung der PM10 Fraktion von Schwebestaub - Referenzmethode und Feldprüfverfahren zu Nachweis der Gleichwertigkeit von Messverfahren und Referenzmethode, Europäisches Komitee für Normung (CEN), Beuth Verlag, Berlin, 1998.

Ding, T., Valkiers, S., Kipphardt, H., De Bievre, P., Taylor, P. D. P., Gonfiantini, R., and Krouse, H. R.: Calibrated sulfur isotope abundance ratios of three IAEA sulfur isotope reference materials and V-CDT with a reassessment of the atomic weight of sulfur, Geochim. Cosmochim. Ac., 65, 2433–2437, 2001.

Draxler, R. R. and Hess, G. D.: An overview of the HYSPLIT_4 modelling system for trajectories, dispersion, and deposition, Aust. Meteorol. Mag., 47, 295–308, 1998.

Draxler, R. R. and Rolph, G. D.: HYSPLIT (HYbrid Single-Particle Lagrangian Integrated Trajectory) Model access via NOAA ARL READY Website: http://www.arl.noaa.gov/ready/hysplit4.

html, NOAA Air Resources Laboratory, Silver Spring, MD, 2003.

Ebert, M., Weinbruch, S., Hoffmann, P., and Ortner, H. M.: Chemical characterization of North Sea aerosol particles, J. Aerosol. Sci., 31 613–632, 2000.

Einsiedl, F., Schäfer, T., and Northrup, P.: Combined sulfur K-edge XANES spectroscopy and stable isotope analyses of fulvic acids and groundwater sulfate identify sulfur cycling in a karstic catchment area, Chem. Geol., 238, 268–276, 2007.

Eriksen, T. E.: Sulfur Isotope-Effects.1. Isotopic-Exchange Coefficient for Sulfur Isotopes $^{34}S^{-32}S^-$ in the System SO_2g-HSO_3^-aq at 25, 35, and 45 Degrees C, Acta Chem. Scand., 26, 573–580, 1972a.

Eriksen, T. E.: Sulfur Isotope-Effects.3. Enrichment of $^{34}S^-$ by Chemical Exchange between SO_2g and Aqueous-Solutions of SO_2, Acta Chem. Scand., 26, 975–979, 1972b.

Foner, H. A. and Ganor, E.: The chemical and mineralogical composition of some urban atmospheric aerosols in Israel, Atmos. Environ., 26, 1083–1093, 1992.

Fowler, D., Muller, J., Smith, R. I., Cape, J. N., and Erisman, J.-W.: Nonlinearities in Source Receptor Relationships for Sulfur and Nitrogen Compounds, Ambio, 34, 41–46, 2005.

Gebauer, G., Giesemann, A., Schulze, E. D., and Jäger, H. J.: Isotope ratios and concentrations of sulfur and nitrogen in needles and soils of Picea abies stands as influenced by atmospheric deposition of sulfur and nitrogen compounds, Plant Soil, 164, 267–281, 1994.

Gröner, E., and Hoppe, P.: Automated ion imaging with the NanoSIMS ion microprobe, Appl. Surf. Sci., 252, 7148–7151, 2006.

Guideline 1999/30/EG: Richtlinie 1999/30/EG des Rates vom 22. April 1999 über Grenzwerte von Schwefeldioxid, Stickstoffdioxid und Stickoxide, Partikel und Blei in der Luft., Amtsblatt Nr. L 163 vom 29.06.1999, 41–60, 1999.

Gwaze, P., Schmid, O., Annegarn, H. J., Andreae, M. O., Huth, J., and Helas, G.: Comparison of three methods of fractal analysis applied to soot aggregates from wood combustion, J. Aerosol. Sci., 37, 820–838, 2006.

Hahne, H.: Zur Verteilung und Genese von Sulfiden in Braunkohlen. Unveröffentlichter Abschlußbericht, Bergakademie Freiberg, 119 pp., 1982.

Hoffman, R. C., Laskin, A., and Finlayson-Pitts, B. J.: Sodium nitrate particles: physical and chemical properties during hydration and dehydration, and implications for aged sea salt aerosols, J. Aerosol Sci., 35, 869–887, 2004.

Hoornaert, S., Van Malderen, H., and van Grieken, R.: Gypsum and other calcium-rich aerosol particles above the North Sea, Environ. Sci. Technol., 30, 1515–1520, 1996.

Hoornaert, S., Godoi, R. H. M., and van Grieken, R.: Single particle characterization of the aerosol in the marine boundary layer and free troposphere over Tenerife, NE Atlantic, during ACE-2, J. Atmos. Chem., 46, 271–293, 2003.

Hoppe, P.: NanoSIMS: A new tool in cosmochemistry, Appl. Surf. Sci., 252, 7102–7106, 2006.

Hoppe, P., Mostefaoui, S., and Stephan, T.: NanoSIMS oxygen and sulfur isotope imaging of primitive solar system materials, Lunar Planet. Sci., 36, abstract #1301 (CD-ROM), 2005.

Hueglin, C., Gehrig, R., Baltensperger, U., Gysel, M., Monn C., and Vonmont, H.: Chemical characterization of $PM_{2.5}$, PM_{10} and coarse Particles at urban, near-city and rural sites in Switzerland, Atmos. Environ., 39, 637–651, 2005.

Hunova, I., Santroch, J., and Ostatnicka, J.: Ambient air quality and deposition trends at rural stations in the Czech Republic during 1993–2001, Atmosp. Environ., 38, 887–989, 2004.

Hwang, H. J. and Ro, C. U.: Direct observation of nitrate and sulfate formations from mineral dust and sea-salts using low-Z particle electron probe X-ray microanalysis, Atmos. Environ., 40, 3869–3880, 2006.

Irwin, J. G., Campbell, G., and Vincent, K.: Trends in sulphate and nitrate wet deposition over the United Kingdom: 1986–1999, Atmos. Environ., 36, 2867–2879, 2002.

Jäger, H. J., Giesemann, A., Krouse, H. R., Legge, A. H., and Esser, J.: Sulphur Isotope Investigation of Atmospheric Sulphur Input to a Terrestrial Ecosystem near Braunschweig, FRG, Angew. Bot., 63, 513–523, 1989.

Klein, H., Wind, P., and van Loon, M.: Transboundary air pollution by main pollutants S, N, O_3 and PM Germany, in: EMEP Assessment Part II: National Contributions, edited by Lövblad, G., Tarrasón, L., Tørseth, K., and Dutchak, S., Oslo, Norwegian Meteorological Institute, 2, 97–108, 2004.

Knöller, K. and Trettin, R.: Isotopenanalytische Bewertung des Sulfathaushaltes in landwirtschaftlich genutzten Wassergewinnungsgebieten, Abschlussbericht Zum Teilprojekt 4 des BMBF-Verbundvorhabens Wasserversorgung und Sulfatbelastung des Grundwassers unter Land- und Forstwirtschaftlich genutzten Flächen, Halle, 2003.

Krouse, H. R. and Grinenko, V. A. (Ed.): Stable isotopes : natural and anthropogenic sulphur in the environment (SCOPE Vol. 43), Wiley, Chichester, 440 pp., 1991.

Krueger, B. J., Grassian, V. H., Cowin, J. P., and Laskin, A.: Heterogeneous chemistry of individual mineral dust particles from different dust source regions: the importance of particle mineralogy), Atmos. Environ., 39, 395–395, 2005.

Kuhlbusch, T., John, A. C., Romazanowa, O., and Top, S.: Identifizierung von PM10-

Emissionsquellen im Rahmen der Maßnahmenplanung zur Reduktion der PM10 Imissionsbelastung in Rheinland-Pfalz. IUTA-Bericht, Institut für Energie und Umweltechnik e.V. (IUTA), Duisburg, 2003.

Landesamt für Umwelt, Wasserwirtschaft und Gewerbeaufsicht Rheinland-Pfalz (08/2005), Monatsbericht 2005 Zentrales Immissionsmessnetz –ZIMEN– 1, available at: http://www.luft-rlp.de, 2005.

Larssen, S., Barrett, K. J., Fiala, J., Goodwin, J., Hagen, L. O., Henriksen, J. F., de Leeuw, F., and Tarrason, L.: Air quality in Europe. State and trends 1990–1999, Topic report 4/2002, 2003.

Laskin, A., Gaspar, D. J., Wang, W. H., Hunt, S. W., Cowin, J. P., Colson, S. D., and Finlayson-Pitts, B. J.: Reactions at interfaces as a source of sulfate formation in sea-salt particles, Science, 301, 340–344, 2003.

Lee, Y. N. and Schwartz, S. E.: Kinetics of oxidation of aqueous sulfur (IV) by nitrogen dioxide. Paper presented at the Fourth International Conference on Precipitation Scavenging, Dry Deposition, and Resuspension, Santa Monica, California, 1982.

Lei, C., Landsberger, S., Basunia, S., and Tao, Y.: Study of $PM_{2.5}$ in Beijing suburban site by neutron activation analysis and source apportionment, J. Radioanal. Nucl. Ch., 261, 87–94, 2004.

Lenschow, P., Abraham, H. J., Kutzner, K., Lutz, M., Preuss, J. D., and Reichenbacher, W.: Some ideas about the sources of PM_{10}, Atmos. Environ., 35, 23–33, 2001.

Li, J., Anderson, J. R., and Buseck, P. R.: TEM study of aerosol particles from clean and polluted marine boundary layers over the North Atlantic, J. Geophys. Res.-Atmos., 108, 4189, doi:10.1029/2002JD002106, 2003.

Lövblad, G., Tarrasón, L., Tørseth, K., Arnell, J., Bartnicki, J., Erisman, J. W., Fagerli, H., Hjelbrekke, A. G., Posch, M., Schaug, J., and Vestreng, V.: Sulphur, in: EMEP Assessment Part I: European Perspective, edited by Lövblad, G., Tarrasón, L., Tørseth, K., and Dutchak, S., Oslo, Norwegian Meteorological Institute, I, 15–45, 2004.

Mamane, Y. and Gottlieb, J.: Nitrate Formation on Sea-Salt and Mineral Particles – a Single-Particle Approach, Atmos. Environ., 26, 1763–1769, 1992.

Mamane, Y., Willis, R., and Conner, T.: Evaluation of computer-controlled scanning electron microscopy applied to an ambient urban aerosol Sample, Aerosol Sci. Technol., 34, 97–107, 2001.

Mayer, B., Feger, K. H., Giesemann, A., and Jäger, H.-J.: Interpretation of sulfur cycling in two catchments in the Black Forest (Germany) using stable sulfur and oxygen isotope data, Biogeochem., 30, 31–58, 1995a.

Mayer, B., Fritz, P., Prietzel, J., and Krouse, H. R.: The use of stable sulfur and oxygen isotope ratios for interpreting the mobility of sulfate in aerobic forest soils, Appl. Geochem. 10, 161–173, 1995b.

McArdle, N. C. and Liss, P. S.: Isotopes and Atmospheric Sulfur, Atmos. Environ., 29, 2553–2556, 1995.

McGee, J. K., Chen, L. C., Cohen, M. D., Chee, G. R., Prophete, C. M., Haykal-Coates, N., Wasson, S. J., Conner, T. L., Costa, D. L., and Gavett, S. H.: Chemical analysis of World Trade Center fine particulate matter for use in toxicologic assessment, Environ. Health Persp., 111, 972–980, 2003.

Niemi, J. V., Tervahattua, H., Virkkulad, A., Hillamod, R., Teinilä, K., Koponene, I. K., and Kulmala, M.: Continental impact on marine boundary layer coarse particles over the Atlantic Ocean between Europe and Antarctica, Atmos. Res., 75, 301–321, 2005.

Novak, M., Kirchner, J. W., Groscheova, H., Havel, M., Cerny, J., Krejci, R., and Buzek, F.: Sulfur isotope dynamics in two Central European watersheds affected by high atmospheric deposition of SO_x, Geochim. Cosmochim. Ac,, 64, 367–383, 2000.

Novak, M., Bottrell, S. H., and Prechova, E.: Sulfur isotope inventories of atmospheric deposition, spruce forest floor and living Sphagnum along a NW-SE transect across Europe, Biogeochem., 53, 23–50, 2001a.

Novak, M., Jackova, I., and Prechova, E.: Temporal Trends in the Isotope Signature of Air-Borne Sulfur in Central Europe, Environ. Sci. Technol., 35, 255–260, 2001b.

Novak, M., Kirchner, J. W., Fottova, D., Prechova, E., Jackova, I., Kram, P., and Hruska, J.: Isotopic evidence for processes of sulfur retention/release in 13 forested catchments spanning a strong pollution gradient (Czech Republic, Central Europe), Global Biogeochem. Cy., 19, GB4012, doi:10.1029/2004GB002396, 2005a.

Novak, M., Vile, M. A., Bottrell, S. H., Stepanova, M., Jackova, I., Buzek, F., Prechova, E., and Newton, R. J.: Isotope systematics of sulfate-oxygen and sulfate-sulfur in six European peatlands, Biogeochem., 76, 187–213, 2005b.

Pakkanen, T., Loukkola, K., Korhonen, C. H., Aurela, M., Mäkelä, T., Hillamo, R. E., Aarnio, P., Koskentalo, T., Kousa, A., and Maenhaut, W.: Sources and chemical composition of atmospheric fine and coarse particles in the Helsinki area, Atmos. Environ., 35, 5381–5391, 2001.

Patris, N., Delmas, R. J., and Jouzel, J.: Isotopic signatures of sulfur in shallow Antarctic ice cores, J. Geophys. Res.-Atmos., 105, 7071–7078, doi:10.1029/1999JD900974, 2000a.

Patris, N., Mihalopoulos, N., Baboukas, E. D., and Jouzel, J.: Isotopic composition of sulfur in size-resolved marine aerosols above the Atlantic Ocean., J. Geophys. Res.-Atmos., 105, 14 449–14 457, doi:10.1029/1999JD901101, 2000b.

Penner, J. E., Andreae, M. O., Annegarn, H., Barrie, L. A., Feichter, J., Hegg, D. A., Jayaraman, A., Leaitch, W. R., Murphy, D., Nganga, J., and Pitari, G.: Aerosols, their direct and indirect effects, in: Climate change 2001: The third assessment report to the intergovernmental panel on climate change, edited by: Houghton, J. T., Ding, Y., Griggset, J., et al., Cambridge University Press, Cambridge, United Kingdom, and New York, USA, 2001.

Pichlmayer, F., Schöner, W., Seibert, P., Stichler, W., and Wagenbacher, D.: Stable Isotope Analysis for Characterization of Pollutants at High Elevation Alpine Sites, Atmos. Environ., 32, 4075–4085, 1998.

Pluta, I.: Identification of mine waters in the southern Upper Silesian Coal Basin (Poland) by δ^{34}S and δ^{18}O, Abstract presented on the Symposium of the International Mine Water Association, Kattowice, Poland, 2002.

Pope, C. A., Bates, D. V., and Raizenne, M. E.: Health-Effects of Particulate Air-Pollution – Time for Reassessment, Environ. Health Persp., 103, 472–480, 1995.

Putaud, J. P., Raes, F., van Dingenen, R., Brüggemann, E., Facchini, M. C., Decesari, S., Fuzzi, S., Gehrig, R., Hüglin, C., Laj, P., Lorbeer, G., Maenhaut, W., Mihalopoulos, N., Müller, K., Querol, X., Rodriguez, S., Schneider, J., Spindler, G., Ten Brink, H. M., Torseth, K., and Wiedensohler, A.: A European aerosol phenomenology – 2: chemical characteristics of particulate matter at kerbside, urban, rural and background sites in Europe, Atmos. Environ., 38, 2579–2595, 2004.

Puxbaum, H., Gomiscek, B., Kalina, M., Bauer, H., Salam, A., Stopper, S., Preining, O., and Hauck, H.: A dual site study of $PM_{2.5}$ and PM_{10} aerosol chemistry in the larger region of Vienna, Austria, Atmos. Environ., 38, 3949–3958, 2004.

Querol, X., Alastuey, A., Chaves, A., Spiro, B., Plana, F., and Lopez-Soler, A.: Sources of natural and anthropogenic sulphur around the Teruel power station, NE Spain. Inferences from sulphur isotope geochemistry, Atmos. Environ., 34, 333–345, 2000.

Ro, C. U., Kim, H., and van Grieken, R.: An expert system for chemical speciation of individual particles using low-Z particle electron probe X-ray microanalysis data, Anal. Chem., 76, 1322–1327, 2004.

Saltzman, E. S., Brass, G., and Price, D.: The mechanism of sulfate aerosol formation: Chemical and sulfur isotopic evidence, Geophys. Res. Lett., 10, 513–516, 1983.

Saul, T. D., Tolocka, M. P., and Johnston, M. V.: Reactive uptake of nitric acid onto sodium chloride aerosols across a wide range of relative humidities, J. Phys. Chem. A, 110, 7614–7620, 2006.

Sievering, H., Boatman, J., Galloway, J., Keene, W., Kim, Y., Luria, M., and Ray, J.: Heterogeneous Sulfur Conversion in Sea-Salt Aerosol-Particles – the Role of Aerosol Water-Content and Size Distribution, Atmos. Environ., 25, 1479–1487, 1991.

Sillanpää, M., Hillamod, R., Saarikoski, S., Frey, A., Pennanen, A., Makkonen, U., Spolnik, Z., van Grieken, R., Branis, M., Brunekreef, B., Chalbot, M. C., Kuhlbusch, T., Sunyer, J., Kerminen, V.-M., and Kulmala, M.: Chemical composition and mass closure of particulate matter at six urban sites in Europe, Atmos. Environ., 40, 212–223, 2006.

Sobanska, S., Coeur, C., Maenhaut, W., and Adams, F.: SEM-EDX Characterization of Tropospheric Aerosols in the Negev Desert (Israel), J. Atmos. Chem., 44, 299–322, 2003.

Spix, C., Heinrich, J., Dockery, D., Schwartz, J., Volksch, G., Schwinkowski, K., Collen, C., and Wichmann, H. E.: Air-Pollution and Daily Mortality in Erfurt, East-Germany, 1980–1989, Environ. Health Persp., 101, 518–526, 1993.

Stoyan, D.: Stochastik für Ingenieure und Naturwissenschaftler, Wiley-VCH, 1998.

Tanaka, N., Rye, D. M., Xiao, Y., and Lasaga, A. C.: Use of Stable Sulfur Isotope Systematics for Evaluating Oxidation Reaction Pathways and in-Cloud Scavenging of Sulfur-Dioxide in the Atmosphere, Geophys. Res. Lett., 21, 1519–1522, doi:10.1029/1994GL00893, 1994.

Thode, H. G., Graham, R. L., and Ziegler, J. A.: A Mass Spectrometer and the Measurement of Isotope Exchange Factors, Canad. J. of Res., B23, 40–47, 1945.

Tichomirowa, M., Bombach, K., and Liebscher, R.: Schwefel- und Sauerstoffisotopenwerte der Atmosphäre in Sachsen: Messungen 2000–2004 und zusammenfassende Interpretation. Wissenschaftliche Mitteilung: Institut für Geologie der TU Bergakademie Freiberg, 27, 73–83, 2004.

Tichomirowa, M., Haubrich, F., Klemm, W., and Matschullat, J.: Regional and temporal (1992-2004) evolution of air-borne sulphur isotope composition in Saxony, southeastern Germany, central Europe, Isotopes Environ. Health Stud., 43, 295–305, 2007.

Torfs, K. M., van Grieken, R., and Buzek, F.: Use of Stable Isotope Measurements to Evaluate the Origin of Sulfur in Gypsum Layers on Limestone Buildings, Environ. Sci. Technol., 31, 2650–2655, 1997.

Vester, B. P.: Feinstaubexposition im urbanen Hintergrundaerosol des Rhein-Main-Gebietes: Ergebnisse aus Einzelpartikelanalyse, Fachbereich Material- und Geowissenschaften, Technische Universität Darmstadt. PhD Thesis, S184, 2006.

Winterholler, B., Hoppe, P., Andreae, M. O., and Foley, S.: Measurement of sulfur isotope ratios in micrometer-sized samples by NanoSIMS, Appl. Surf. Sci., 252, 7128–7131, 2006.

Winterholler, B., Hoppe, P., Foley, S., and Andreae, M. O.: Sulfur isotope ratio measurements of individual sulfate particles by NanoSIMS, Int. J. Mass Spectrom., 272, 63–77, doi:10.1016/j.ijms.2008.01.003, 2008.

Xhoffer, C., Bernard, P., van Grieken, R., and van der Auwera, L.: Chemical characterization and source apportionment of individual aerosol-particles over the North-Sea and the English-Channel using multivariate techniques, Environ. Sci. Technol., 25, 1470–1478, 1991.

Zhao, F. J., Knights, J. S., Hu, Z. Y., and McGrath, S. P.: Stable Sulfur Isotope Ratio Indicates Long-Term Changes in Sulfur Deposition in the Broadbalk Experiment since 1845, J. Environ. Qual., 32, 33–39, 2003.

Zhuang, H., Chan, C. K., Fang, M., and Wexler, A. S.: Formation of nitrate and non sea salt sulfate on coarse particles, Atmos. Environ., 33, 4223–4233, 1999.

Table 1. δ^{34}S values of coal, oil, slag fly ash and SO_2 emissions of power plants in Europe.

	Coal	Fly ash	inlet gas	SO_2 emissions	product
Power plants					
Belachtow (Poland)[1]	∼+8‰		−1.33‰ ±0.03‰ [A]	−4.88‰ ±0.03‰ [A]	+1.21‰ ±0.03‰ [A]
Laziska (Poland)[2]		+4.60‰ [A]			+1.22‰ [A]
Rybnik (Poland)[2]		+4.31‰ [A]			−0.5‰ ±1.91‰ [A]
Bielsko-Biala (Poland)[2]		+3.82‰ [A]			
Czechowice-Dziedzice (Poland)[2]					−2.71‰ [A]
Chvaletice (Czech Republic)[3]	−1.0‰			−0.9‰ [B]	
Sostanj (Slovakia)[4]	+8.1‰			8.4‰ [B]	
Trbovlje (Slovakia)[4]	+11.2‰			+14.3‰ [B]	
Tereul (Spain)[5]		+1.0‰ [B]		−0.9‰ [B]	
Black triangle[6]				+6‰ [B]	
Coals					
Hambach (France)[7]	+3.3‰				
Yanowice (Poland)[7]	+4.0‰				
Sosnica (Poland)[2]	−2.5‰ to +8.6‰				
Brown coal middle Germany Province[8]	+4.7‰ to +11.9‰				
Crude oil[9]	−10‰ to +10‰				

[A] Flue gas desulfurization: inlet gas = gas measured before desulfurization, SO_2 emission = gas emitted after desulfurization, product = solid waste (sulfate) produced during the desulfuization prozess;

[B] no flue gas desulfurization;

[1] Derda and Chmielewski, 2003;

[2] Pluta, 2002;

[3] Buzek et al., 1991;

[4] Bericnik-Vrbovsek et al., 2002;

[5] Querol et al., 2000;

[6] Pichlmayer et al., 1998;

[7] Zhao et al., 2003;

[8] Hahne 1982;

[9] Krouse and Grinenko, 1991

Table 2. Summary of meteorological data for samples collected in Mainz during August 2005. Meteorological data was downloaded from http://www.luft-rlp.de. *T* is the average daily temperature.

sample	date	flow l min^{-1}	sample volume m^3	windspeed m s^{-1}	T °C	RH$_{min}$ %	RH$_{max}$ %	precipit. mm	
#1	2.8.–3.8.	16	22.1	1.9	19	45	95	1.6	sunny
#2	3.8.–4.8.	20	27.0	2.0	19	34	80	0.4	sunny
#3	4.8.–5.8.	20	27.6	1.7	17	39	95	0.2	sunny
#4	17.8.–18.8.	15	23.0	1.6	22	38	88	0	sunny
#5	18.8.–19.8.	15	19.2	1.6	21	40	96	0.1	sunny
#6	19.8.–20.8.	10	14.1	1.4	19	47	98	0.1	sunny
#7	20.8.–22.8.	10	25.8	2.0	19	47	90	0	sunny/cloudy
#8	22.8.–23.8.	10	15.5	2.3	20	49	90	0	sunny

Table 3. Comparison of PM_{10} and $PM_{2.5}$ calculated from single particle analysis with PM_{10}, $PM_{2.5}$ and SO_2 or soot (all reported in $\mu g\,m^{-3}$) at several measurement stations in Mainz. Data for the measurement stations in Mainz were downloaded from http://www.luft-rlp.de.

Sample	MPI		Mombach		Goetheplatz		Zitadelle		Paracelsusstr.		
	PM_{10}	$PM_{2.5}$	PM_{10}	SO_2	PM_{10}	SO_2	PM_{10}	$PM_{2.5}$	SO_2	PM_{10}	soot
Sample 1	4	1.2	13	2.3	15	2.7	15	11	1.9	23	3.3
Sample 2	4	2	13	2.3	13	2.7	15	12	2.3	25	2.9
Sample 3			13	2.3	15	2.3	18	13	2.3	29	2.9
Sample 4	9	3.3	21	2.3	24	2.3	26	20	2.3	35	4.0
Sample 5	12	3.1	24	2.3	27	2.7	30	23	2.3	42	4.5
Sample 6			19	1.9	20	2.7	22	19	1.9	35	4.3
Sample 7	6	1.9	17	1.5	20	2.0	22	21	1.5	30	4.1
Sample 8	7	3.1	23	2.3	27	2.7	28	25	1.9	42	2.6

Table 4. Instrumental mass fractionation factors for $^{34}S/^{32}S$ measured with the NanoSIMS and average diameter of the standard particles on which instrumental mass fractionation was determined. When the instrumental mass fractionation is determined on particles pressed into gold substrate, no grain size correction is necessary. $BaSO_{4true}$ is the calibrated isotope ratio of $BaSO_4$ based on delta values of 0.5‰ for IAEA SO-5 and –34.2‰ for IAEA SO-6 and a $n(^{34}S)/n(^{32}S))_{VCDT}$=0.044163 (Ding et al., 2001). $BaSO_{4SIMS}$ is the measured $N(^{34}S)/N(^{32}S)$)-ratio measured by SIMS.

Session	$\frac{BaSO_{4true}}{BaSO_{4SIMS}}$	σ	$D_{P,m}$ [μm]	Substrate
11/2005	1.0148	0.0012	3.2	Filter
10/2005	1.0106	0.0005		Gold
09/2005	1.0122	0.0006		Gold
08/2005	1.0317	0.0008	3.6	Filter

Table 5. Average semi-quantitative composition of different particle groups in wheight %. Group 1 sea salt is missing, as no particles of this group were encountered in samples collected in Mainz. N_a: Number of particles analyzed in the respective Group. Element concentrations are semi-quantitative. The total counts of the EDX spectrum were normalized to 100% after background correction and used to estimate the semi-quantitative composition of the particles. Oxygen and carbon are present in the filter substrate and were not analyzed. S is assumed to be SO_4 and Si is assumed to be SiO_2. Cation concentrations close to 100% indicate carbonates, oxides or oxyhydroxides.

	Group	N_a	N	Fe	Na	SiO_2	P	SO_4	Cl	K	Ca
Aged sea salt	2	97	4	<1	26	14	n.d.	26	21	5	3
Quartz and silicates	3	1312	<1	4	3	88	<1	n.d.	<1	3	3
Silicates + sulfate coating	3a	123	<1	2	7	51	n.d.	28	<1	5	6
Silicates + nitrate coating	3b	144	8	3	13	39	n.d.	n.d.	13	1	16
Ammonium (bi) sulfate	4a,b	787	2	<1	n.d.	<1	n.d.	97	<1	<1	<1
Gypsum	5	404	<1	<1	<1	<1	n.d.	73	<1	<1	27
Mixed sulfates	6	140	4	4	19	1	1	33	<1	32	3
Calcite/Gypsum	7	101	<1	<1	n.d.	<1	n.d.	n.d.	<1	<1	99
Fe-Oxides	8	17	<1	98	n.d.	<1	n.a.	n.d.	<1	n.d.	<1
Others	9	1082	9	3	52	<1	4	n.d.	4	16	14
Image analysis only	10	1338	<1	<1	<1	<1	<1	<1	<1	<1	<1

n.d. – not detected.
n.a. – not analysed.

Table 6. Sample composition in % of total particle number (N_a) calculated from single particle analysis in the SEM. Results are given for three size ranges: Particles below the detection limit of the image analysis (<1 μm), particles 1–3 μm and coarse mode particles >3 μm. Ammonium sulfate is usually underestimated by single particle analysis. Particle numbers are estimated based on bulk analysis of the respective samples.

	Group Sample	#1	#2	#4	#5	#7	#8
< 1 μm							
Aged sea salt+S	2	2.2	5.9	0.2	0	0	0
Quartz and silicates	3	3.2	15.4	28.4	40.2	41.8	0
Silicates + sulfur coating	3a	1.1	1.1	2.6	3.3	5.2	0
Silicates + nitrate coating	3b	0	0.9	3.7	8.6	1.7	0
Ammonium(bi)sulfate	4	15.9	45.1	11.9	4.2	16.1	18
Gypsum	5	4.8	4.4	23.3	11.5	13.8	29
Mixed sulfates	6	8.5	2.8	0.9	0.3	1.4	0
Calcite/Dolomite	7	0	1.4	2.2	7.4	0.6	24
Fe-Oxides/Hydroxides	8	0	0	0.4	0.6	0	0
Others	9	63.5	23.0	26.4	24.0	19.3	29
Image analysis only	10	n.a.	n.a.	n.a.	n.a.	n.a.	n.a.
N_a		189	884	455	338	347	17

Table 6. Continued.

	Group Sample	#1	#2	#4	#5	#7	#8
1–3 μm							
Aged sea salt+S	2	0.7	2.7	0	0	0	0
Quartz and silicates	3	2.2	4.1	8.1	25.3	27.6	13
Silicates + sulfur coating	3a	0.7	0	1.0	0.4	6.9	0
Silicates + nitrate coating	3b	0	0.5	0	2.7	2.3	0
Ammonium(bi)sulfate	4	4.3	19.0	15.2	6.1	5.7	13
Gypsum	5	1.4	2.7	18.7	3.4	17.2	50
Mixed sulfates	6	8.7	0.9	1.5	3.8	5.7	0
Calcite/Dolomite	7	0.7	0.5	0.5	5.4	0	0
Fe-Oxides/Hydroxides	8	0	0	0.5	0	0	0
Others	9	13.8	14.5	14.1	32.2	5.7	13
Image analysis only	10	67.4	55.2	40.4	20.7	28.7	13
N_a		138	221	198	261	87	8

Table 6. Continued.

	Group Sample	#1	#2	#4	#5	#7	#8
>3 µm							
Aged sea salt+S	2	2.4	3.6	0	0.6	1.0	0
Quartz and silicates	3	20.9	9.3	26.8	41.0	26.4	19
Silicates + sulfur coating	3a	1.6	0.5	2.0	4.6	10.7	11
Silicates + nitrate coating	3b	0.4	0	2.4	4.4	1.0	4
Ammonium(bi)sulfate	4	5.9	8.8	6.1	1.7	6.1	17
Gypsum	5	0.8	3.4	5.4	1.9	4.1	26
Mixed sulfates	6	3.5	1.4	0.4	3.6	4.6	0
Calcite/Dolomite	7	3.1	1.1	1.1	1.0	1.0	2
Fe-Oxides/Hydroxides	8	0	0	0.6	1.0	0.5	0
Others	9	23.9	9.3	10.7	15.5	10.1	2
Image analysis only	10	37.6	62.5	44.5	24.6	34.8	19
N_a		255	557	541	804	197	47

Table 7. δ^{34}S values of different particle types in different samples. The semi-quantitative chemical composition was characterized by EDX. Primary and secondary gypsum particles and silicates and fly ash were distinguished based on particle morphology during manual SEM analysis. The δ^{34}S of individual particles was measured by NanoSIMS. Errors are 1σ and include the standard deviation of the isotopic composition caused by the presence of different oxidation pathways/different sources in separate particles within the same particle group (i.e., the error of the weighted mean is multiplied by $\sqrt{(\chi^2)}$ for $\chi^2>1$) and, therefore, includes the natural variability of the sample. The error of an individual analysis is typically 7‰ due to inherent limitations in the grain-to-grain reproducibility and the counting statistical limitations imposed by small grains. Errors <7‰ indicate a very low natural variability between different particles in the same group. Errors >7‰ indicate large differences between different particles in the same group, e.g., pollen grains in Sample 1. f_{SO_4}: fraction of total sulfate mass contributed by the respective group.

Group	Sample 1		Sample 2		Sample 4		Sample 5		Sample 7		Sample 8	
	δ^{34}S [‰]	f_{SO_4}	δ^{34}S [‰]	f_{SO_4}	δ^{34}S [‰]	f_{SO_4}	δ^{34}S [‰]	f_{SO_4}	δ^{34}S [‰]	f_{SO_4}	δ^{34}S [‰]	f_{SO_4}
Isotopic signature of secondary particles												
#2	12±7	0.038		0.028		0.001		0.045		0.034		0.036
#3a	9±5	0.060		0.005	1±2	0.048	8±3	0.096	11±5	0.134	10±7	0.083
#4a	−16±5	0.198	2±3	0.404	−10±2	0.086	−15±5	0.024	2±3	0.071		0.039
#4b	15±6	0.361	19±4	0.208	1±4	0.360	3±3	0.281	16±2	0.225	7±4	0.282
#5	17±4	0.142	24±9	0.306	12±3	0.452	1±3	0.211	16±1	0.439	10±5	0.560
#6	22±2	0.185	12±12	0.033	7±4	0.037	6±6	0.320	9±3	0.086		0
$\delta^{34}S_{bulk}$	10±4		13±7		5±3		3±7		14±4		8±7	
$\delta^{34}S_{nsss}$	10±4		13±7		5±3		3±7		14±4		8±7	
$\delta^{34}S_{SO_2}$	−7±5		11±3		−1±2		−6±5		11±3			
Isotopic signature of primary particles												
Ca-Posphate							23±5					
Group 5										16±4		
Group 5										15±4		
Group 5										21±4		
Fly ash									25±5			
Pollen	9±10	0.016	19±7	0.013		0.015	18±3	0.020	26±5	0.012		0.001
SO_4^{2-} [μg m^{-3}]		0.426		1.353		2.222		1.431		1.388		3.303
f_{nsss}		0.987		0.973		1.000		0.978		0.999		0.998

Table 8. Details of all aerosol particles analyzed by single particle analysis.

Grain_spot	$^{34}S/^{32}S$	$\pm 1\sigma$	$\delta^{34}S$ [‰]	$\pm 1\sigma$ [‰]	group	description	diameter [μm]
Filter 1: 2.–3. August							
20050808_8	0.0439	0.0001	32	7	6	dried droplet mixed sulfate needles	0.6–1.3
20050808_10	0.0433	0.0003	18	9	6	dried droplet mixed sulfate needles	1.1
20050808_11	0.0434	0.0002	24	7	6	dried droplet mixed sulfates	2.8
20050808_15	0.0434	0.0002	23	7	5	dried droplet + Gypsum needle	2.1
20050808_16	0.0429	0.0001	13	7	3a	sulfates on silicate	7.7
20050808_17	0.0426	0.0001	2	7	6	mixed sulfates	3.1
20050808_18	0.0429	0.0002	31	8	9	plant depris + secondary gypsum	12.5
20050808_19	0.0435	0.0001	25	7	6	dried droplet mixed sulfate needles	0.7–2.1
20050808_21	0.0422	0.0002	−14	7	4a		1.2
20050808_22	0.0425	0.0003	−6	8	4a		
20050808_27	0.0434	0.0001	21	7	6	dried droplet + secondary gypsum	1.1
20050808_28	0.0434	0.0001	19	6	5	dried droplet + secondary gypsum	1.6
20050808_29	0.0412	0.0002	−35	7	4a		
20050808_30	0.0424	0.0002	0	7	6	dried droplet mixed sulfates	2.8
20050808_31	0.0435	0.0002	21	7	6	dried droplet	0.2
20050808_32	0.0425	0.0001	9	6	9	biological particles	5.2
20050808_33	0.0431	0.0001	24	6	6	dried droplet mixed sulfates	6.1
20050808_35	0.0427	0.0002	7	8	5	gypsum	3.5
20050808_36	0.0421	0.0001	−4	6	9	pollen	3.6
20050808_37	0.0430	0.0001	6	6	3a	coating on soot/silicate particle	2.7
20050808_41	0.0429	0.0001	12	7	2	gypsum/Halite/sodium sulfate	2.5
20050808_42	0.0431	0.0001	24	6	6	dried droplet mixed sulfates	6.7
20050808_45	0.0441	0.0001	37	7	6	mixed sulfate needles	1.8
20050808_46	0.0423	0.0001	−4	7	4a		
20050808_47	0.0434	0.001	29	6	6	iron oxides + secondary gypsum	5.0
20050808_48	0.0432	0.0001	15	6	4b	dried droplet	1.8
20050808_49	0.0434	0.0001	25	7	6	dried droplet	3.1
20050808_50	0.0425	0.0002	−5	7	4a		
20050808_52	0.0417	0.0001	−28	7	4a		

Table 8. Continued.

Grain_spot	^{34}S/^{32}S	±1σ	δ^{34}S [‰]	±1σ [‰]	group description		diameter [μm]
Filter 2: 3.–4. August							
20050808_63	0.04212	0.0002	−10	6	4a	secondary particle	2.5
20050808_64	0.04248	0.0001	−5	6	4a	secondary particle	<1
20050808_65	0.04323	0.0001	38	6	9	biological particles	18.2
20050808_66	0.04336	0.0002	16	6	4a	secondary particle	<1
20050808_68	0.04350	0.0001	22	6	6	secondary particle	1.9
20050808_69	0.04250	0.0002	−3	6	4a	secondary particle	1.1
20050808_71	0.04275	0.0001	7	6	9	biological particles	6.8
20050808_72	0.04347	0.0001	24	6	4b	secondary particle	3.5
20050808_73	0.04303	0.0002	8	6	4a	secondary particle	<1
20050808_74	0.04269	0.0002	37	6	5	dried droplet	21.5
20050808_75	0.04290	0.0001	23	6	9	biological particles	10
20050808_76	0.04280	0.0003	14	6	4b	mixed sulfates	7.3
20050808_77	0.04338	0.0001	19	6	4b	secondary particle	5.0
20050808_78	0.04210	0.0002	7	6	9	mixed sulfates/silicate	9.7
200511_23	0.04405	0.0001	15	6	4a	not identified	<1
4@2	0.04359	0.0002	0	7	4a	secondary particle	<1
4@3	0.04334	0.0002	−6	7	4a	secondary particle	<1
200511_28	0.04350	0.0002	2	7	4a	dried droplets	2.5
200511_29	0.04350	0.0002	33	9	5	gypsum, secondary particle	7.5
200511_31	0.04431	0.0001	39	6	5	gypsum ,secondary particle	<1

Table 8. Continued.

Grain_spot	$^{34}S/^{32}S$	$\pm 1\sigma$	$\delta^{34}S$ [‰]	$\pm 1\sigma$ [‰]	group	description	diameter [μm]
Filter 4: 17.–18. August							
200510_8	0.04384	0.0003	18	7	5	gypsum. secondary particle	3.1
200510_9	0.04344	0.0002	4	6	5	gypsum, secondary particle	<1
200510_10	0.04447	0.0003	28	7	5	gypsum, secondary particle	<1
200510_11	0.04288	0.0001	−12	4	4a	secondary particle	2.3
200510_12	0.04315	0.0002	−9	6	3a	silicate with coating	<1
200510_15	0.04301	0.0001	−12	4	4a	secondary particle	<1
200510_16	0.04364	0.0001	7	4	4b	secondary particle	<1
200510_17	0.04319	0.0001	−8	3	4a	secondary particle	<1
200510_19	0.04404	0.0001	18	3	5	gypsum, secondary particle	<1
200510_20	0.04356	0.0002	1	4	4b	secondary particle	<1
200510_21	0.04286	0.0002	−9	6	5	gypsum, secondary particle	<1
200510_22	0.04374	0.0002	11	5	5	gypsum, secondary particle	<1
200510_23	0.04381	0.0001	13	4	5	gypsum, secondary particle	<1
200510_24	0.04368	0.0001	4	3	3a	silicate with coating	<1
200510_25	0.04389	0.0002	15	5	5	gypusm, secondary particle	<1
200510_26	0.04352	0.0001	2	4	3a	silicate with coating	1.4
200510_27	0.04369	0.0002	6	5	3a	silicate with coating	1.8
200510_28	0.04321	0.0001	−2	4	3a	silicate with coating	3.7
200510_35	0.04367	0.0002	9	5	5	gypsum, secondary particle	<1
200510_36	0.04358	0.0002	7	4	5	gypsum, secondary particle	<1

Table 8. Continued.

Grain_spot	$^{34}S/^{32}S$	±1σ	$\delta^{34}S$ [‰]	±1σ [‰]	group	description	diameter [μm]
Filter 5: 18.–19. August							
20050830_42	0.04368	0.0001	11	5	5	gypsum, secondary particle	<1
20050830_44	0.04287	0.0003	−13	7	6	secondary particle	<1
20050830_46	0.04309	0.0001	−2	5	5	gypsum, secondary particle	<1
20050830_47	0.04313	0.0002	−1	6	5	gypsum, secondary particle	<1
20050830_48	0.04313	0.0001	2	5	3a	silicate with coating +sec. particle	2.4
20050830_49	0.04266	0.0002	−17	6	4a	secondary particle	<1
20050830_50	0.04300	0.0001	16	4	3a	silicate with coating	12.7
20050830_51	0.04283	0.0001	−4	5	6	secondary particle	2.6
20050830_52	0.04321	0.0001	−3	5	3a	iron oxide + sulfate coating	1.8
20050830_53	0.04339	0.0001	17	5	3a	silicate with coating	9.2
20050830_53	0.04240	0.0001	−1	5	6	Na$^-$ sulfate	10.1
20050830_56	0.04323	0.0001	23	5	6	Ca-phosphate/sulfate	13.6
20050830_57	0.04316	0.0001	19	4	9	biological particles + secondary particles	10.4
20050830_58	0.04330	0.0001	3	5	5	gypsum, secondary particle	<1
20050830_59	0.04261	0.0001	−13	5			<1
20050830_60	0.04274	0.0001	−10	5			<1
20050830_61	0.04352	0.0002	9	5	3a	silicate with coating	1.3
20050830_62	0.04349	0.0001	1	5	4b	secondary particle	<1
20050830_63	0.04343	0.0001	17	4	9	pollen	4.5
20050830_64	0.04341	0.0001	−1	5	4b	secondary particle	<1
20050830_65	0.04329	0.0001	−4	5	4a	secondary particle	<1
20050830_66	0.04387	0.0001	16	5	5	gypsum, secondary particle	<1
20050830_68	0.04378	0.0002	7	6	4b	secondary particle	<1
20050830_69	0.04306	0.0001	−3	5	5	gypsum, secondary particle	<1
20050830_71	0.04352	0.0002	8	5	5	gypsum, secondary particle	<1
200511_21	0.04400	0.0001	12	6	4b	secondary particle	<1
200511_22	0.04397	0.0002	12	6	4b	secondary particle	<1

Table 8. Continued.

Grain_spot	$^{34}S/^{32}S$	±1σ	$\delta^{34}S$ [‰]	±1σ [‰]	group description		diameter [μm]
Filter 7: 20.–22. August							
20050830_5	0.04316	0.0001	1	4	3a	silicate with coating	5.0
20050830_6	0.04286	0.0001	−11	5	4a	secondary particle	2.2
20050830_7	0.04332	0.0001	9	4	3a	silicate with coating	7.5
20050830_8	0.04367	0.0001	16	4	5	gypsum primary	3.2
20050830_9	0.04363	0.0001	3	5	4a	secondary particle	<1
sple@6	0.04397	0.0001	20	5	5	iron oxide + secondary gypsum	1.5
sple@2	0.04364	0.0001	15	4	5	gypsum primary	3.2
sple@3	0.04377	0.0001	10	5	4b	secondary particle	1.9
sple@4	0.04356	0.0001	10	4	6	secondary particle	<1
20050830_11	0.04375	0.0002	13	6	5	secondary gypsum	<1
20050830_12	0.04360	0.0002	9	6	5	secondary gypsum	<1
20050830_13	0.04387	0.0003	9	7	4a	secondary particle	<1
20050830_14	0.04433	0.0001	26	5	5	thin layer of secondary gypsum	6.5
20050830_15	0.04417	0.0001	22	4	5	thin layer of secondary gypsum	4.6
20050830_16	0.04360	0.0001	26	5	9	pollen	8.0
20050830_17	0.04416	0.0002	25	6	5	secondary gypsum	1.9
20050830_18	0.04430	0.0001	28	4	5	iron oxide + sulfur coating	1.5
20050830_19	0.04392	0.0001	17	5	5	secondary gypsum	<1
20050830_21	0.04366	0.0001	21	4	5	primary gypsum + silicate	6.2
20050830_22	0.04359	0.0001	10	4	5	secondary gypsum	<1
20050830_23	0.04369	0.0001	12	5	5	secondary gypsum	<1
20050830_24	0.04365	0.0001	24	5	5	coating on silicate particle	8.1
20050830_26	0.04389	0.0002	18	6	5	secondary gypsum	1.4
20050830_27	0.04410	0.0003	15	7	4b	secondary particle	<1
20050830_28	0.04407	0.0002	20	6	5	secondary gypsum	<1
20050830_29	0.04441	0.0003	22	7	4b	secondary particle	<1
20050830_30	0.04352	0.0001	12	5	6	carbon, oxygen, extremely hard	6.5
20050830_31	0.04443	0.0001	30	5	3a	coating on silicate	5.2
20050830_32	0.04426	0.0001	20	5	4b	gypsum + ammonium silicate	1.2
20050830_33	0.04346	0.0001	7	5	3a	coating on silicate	4.8
20050830_34	0.04356	0.0001	13	5	3a	coating on silicate	6.9
20050830_35	0.04415	0.0001	25	5	6	coating on silicate	1.8
200511_15	0.04371	0.0002	3	7	4a	secondary particle	1.4
200511_16	0.04366	0.0002	8	7	5	secondary gypsum	<1
200511_17	0.04349	0.0001	−2	6	4a	secondary particle	<1
200511_18	0.04383	0.0002	7	7	4a	secondary particle	1.0
200511_19	0.04350	0.0001	4	6	6	secondary particle	<1
200511_20	0.04347	0.0001	4	6	5	secondary gypsum	<1

Table 8. Continued.

Grain_spot	$^{34}S/^{32}S$	±1σ	$\delta^{34}S$ [‰]	±1σ [‰]	group description		diameter [μm]
Filter 8: 22.–23. August							
200511_6	0.04366	0.0001	9	6	4b	ammonium sulfate	4.9
200511_7	0.04377	0.0001	22	6	3a	silicate	7.3
200511_8	0.04386	0.0001	13	6	4b	ammonium sulfate	4.5
200511_9	0.04342	0.0001	5	6	5	gypsum needle	1.4
sample@1	0.04285	0.0002	3	7	3a	ammonium sulfate + silicate	12.7
sample@2	0.04351	0.0001	9	6	4b	ammonium sulfate	6.9
sample@3	0.04193	0.0001	−15	6	4b	gypsum + ammonium sulfate	12.7
sample@4	0.04352	0.0001	7	6	5	gypsum needle	1.8
200511_10	0.04372	0.0001	11	6	5	secondary gypsum	1.4
200511_11	0.04401	0.0001	17	6	6	secondary mixed sulfate	2.7
200511_12	0.04370	0.0001	11	6	4b	ammonium sulfate	5.3
sample@5	0.04410	0.0001	27	6	5	large gypsum needle	5.5
sample@6	0.04343	0.0002	2	7	6	secondary particles	1.9
sample@7	0.04307	0.0002	−1	7	3a	gypsum needle and silicate particle	3.1
sample@8	0.04308	0.0001	−2	6	5	gypsum needle	1.9
sample@9	0.04374	0.0003	13	9	4b	coarse mode ammonium sulfate	5.8

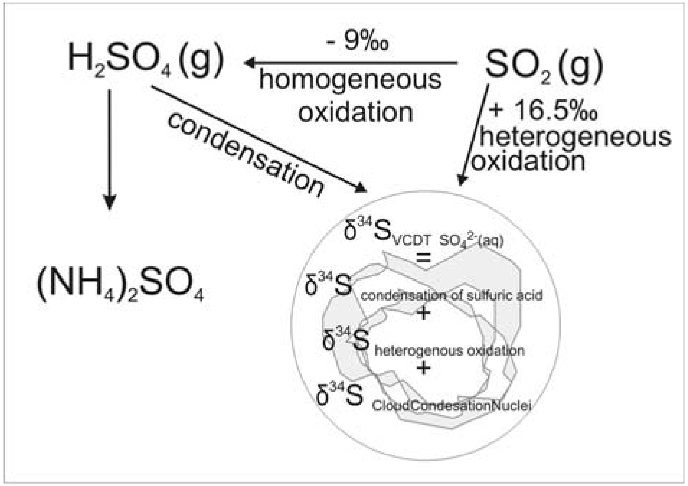

Fig. 1. The sulfur isotopic signature of the source SO_2 is changed during homogeneous (gas phase) and heterogeneous (aqueous phase) oxidation. Provided that the isotopic composition of source SO_2 is known and no water-soluble primary sulfate acted as cloud condensation nuclei, the relative contribution of condensations of gaseous sulfuric acid onto the droplet and heterogeneous oxidation in the droplet can be calculated. The isotopic composition of source SO_2 can be estimated from particles that derive from gas to particle conversion, such as fine mode ammonium sulfate.

Title Page
Abstract
Introduction
Conclusions
References
Tables
Figures
◀|
|▶
◀
▶
Back
Close
Full Screen / Esc
Printer-friendly Version
Interactive Discussion

Fig. 2. Overview over the sampling location and major stationary sources of aerosol particles and SO_2 in Mainz (Map courtesy of Google Earth^{TM} maping service). The geographic coordingates are: MPI Mainz 49°59′31″ N, 8°14′15″ O; Mainz University 49°59′32″ N, 8°14′28″ O; Goetheplatz 50°00′38″ N, 8°15′15″ O; Parcus Strasse 50°00′04″ N, 8°15′40″ O; Zitadelle 49°59′36″ N, 8°16′27″ O; Mombach 50°01’06″ N, 8°13′13″ O; cement works 50°02′53″ N, 8°16′12″ O and 49°58′24″ N, 8°19′03″ O; limestone mine 49°58′07″ N, 8°17′56″ O; municipal waste incineration plant 50°01′35″ N, 8°14′16″ O; gas fired power plant 50°01′33″ N, 8°14′14″ O; glass production 50°01′23″ N, 8°14′24″ O and 50°01′56″ N, 8°14′52″ O; coffe roasting 50°01′38″ N, 8°13′34″ O.

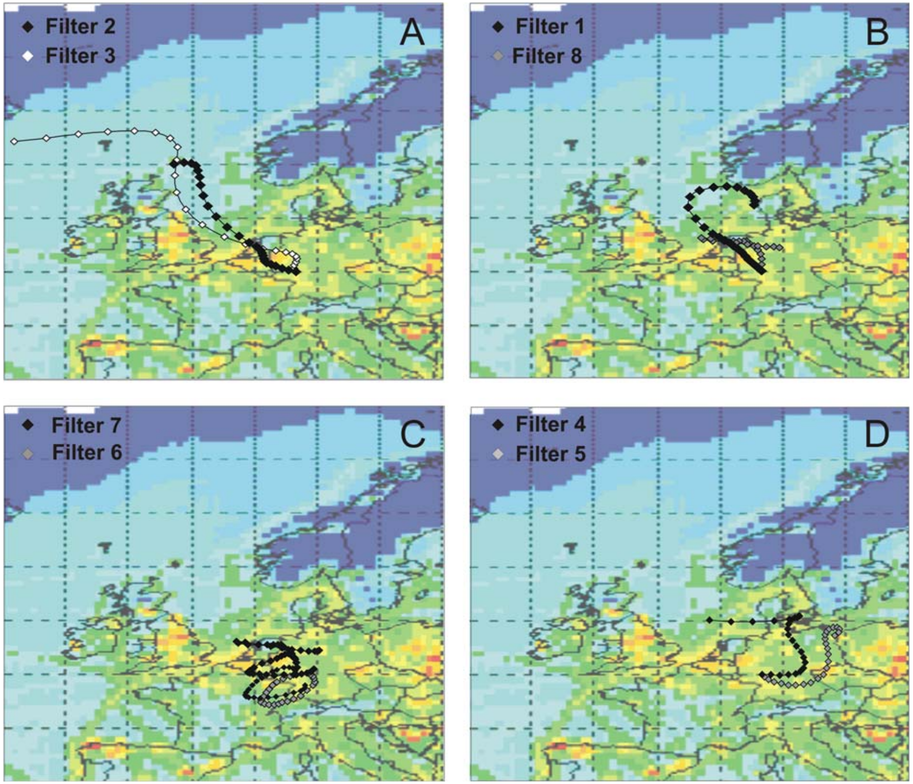

Fig. 3. **(a)** Samples with backward trajectories reaching Mainz from the north and north-west that show no signs of extensive in-cloud processing. **(b)** Samples with backward trajectories reaching Mainz from the north and north-west that show strong signs of in-cloud processing such as dried droplets, long secondary needles and coarse-mode ammonium sulfate particles. **(c)** Samples with backward trajectories reaching Mainz from west to north-west. **(d)** Samples with backward trajectories reaching Mainz from the east.

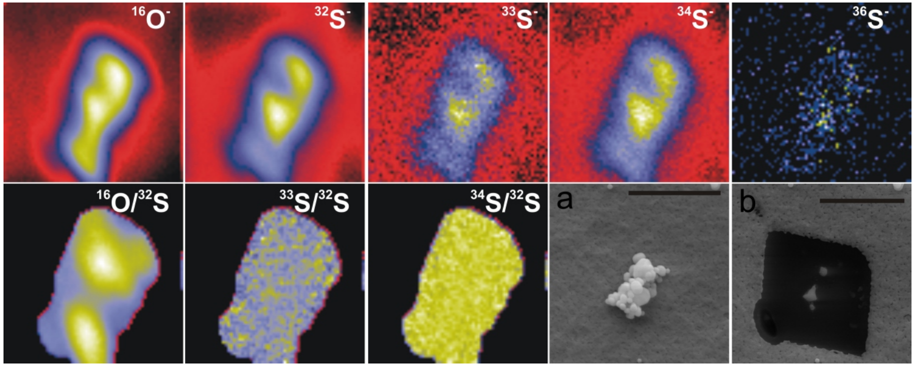

Fig. 4. $BaSO_4$ standard grain illustrating the analytical procedure. Particles are documented with help of the SEM before **(a)** and after SIMS analysis **(b)**. SEM conditions: EHT 10 keV, WD 9 mm, scale bar 2 μm. SIMS conditions: Field of view 2 μm×2 μm, simultaneous collection of $^{16}O^-$, $^{32}S^-$, $^{33}S^-$, $^{34}S^-$ and $^{36}S^-$, Cs^+ primary ions, 1 pA primary current, 100 nm beam diameter. The black square on SEM image (b) is the area were the filter material was sputtered away during analysis and indicates the exact position of the SIMS measurement field.

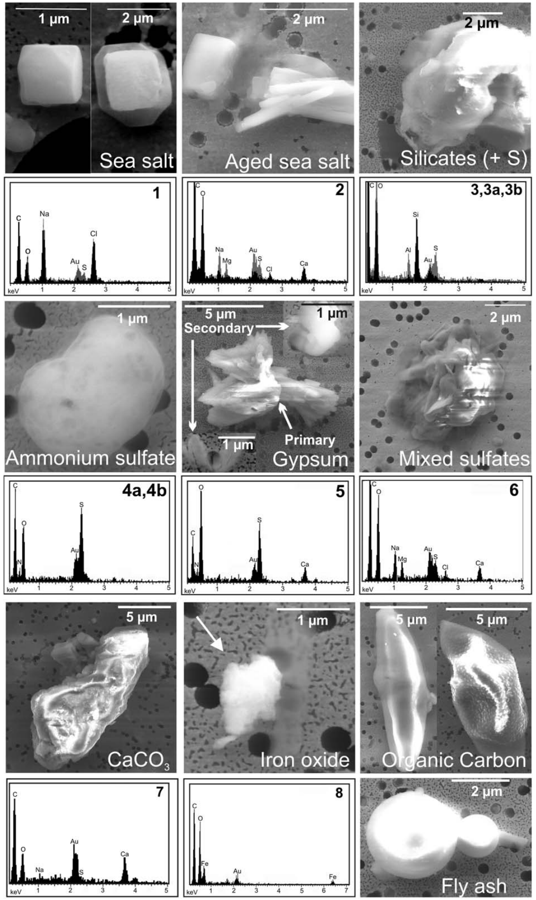

Fig. 5. SEM images and typical EDX spectra for all particle groups (except 9 and 10) and images of selected primary particle.

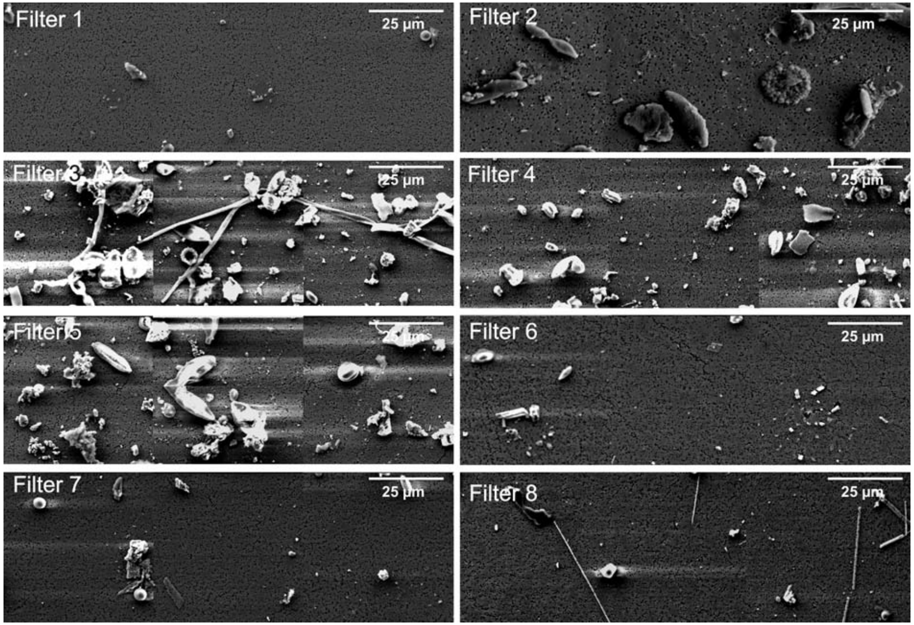

Fig. 6. Overview over all samples. SEM conditions: EHT 10 keV, working distance 9 mm. Scale bars are 25 μm.

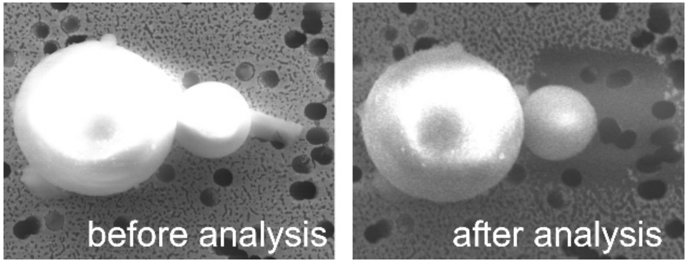

Fig. 7. Fly ash particles before and after SEM analysis. Working distance 11 mm, EHT 10 keV. The black square on the right SEM image is the area was the filter material was sputtered away during analysis and indicates the exact position of the measurement field. The gypsum needle associated with the fly ash was sputtered away completely, while the rest of the fly ash was resistant enough to survive analysis.

Title Page
Abstract
Introduction
Conclusions
References
Tables
Figures
◀◀
▶▶
◀
▶
Back
Close
Full Screen / Esc
Printer-friendly Version
Interactive Discussion

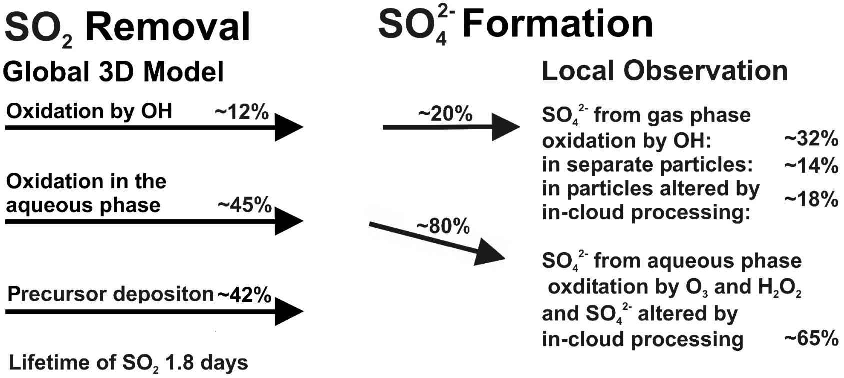

Fig. 8. Relative contribution of different oxidation pathways and precursor deposition to SO_2 removal. The annual average of 12 global 3-D models (Penner et al., 2001) is compared with the relative contribution of gas phase and aqueous phase oxidation on mostly sunny August days in Mainz. Approximately 3% of SO_4^{2-} is found in primary particles.

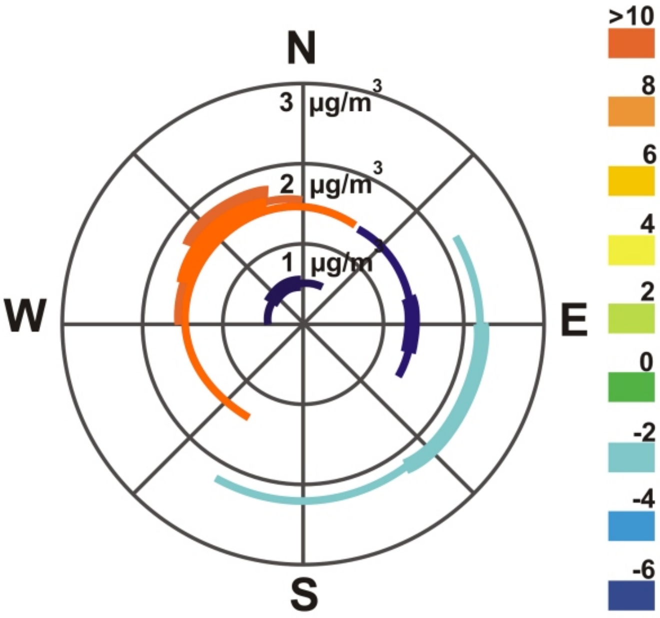

Fig. 9. Dependence of δ^{34}S of source SO_2 on the wind direction.